Ore Geology Reviews 78 (2016) 388–408

Contents lists available at ScienceDirect

Ore Geology Reviews

journal homepage: www.elsevier.com/locate/oregeorev

Partial least squares-discriminant analysis of trace element compositions of magnetite from various VMS deposit subtypes: Application to mineral exploration

Sheida Makvandi [a], Massoud Ghasemzadeh-Barvarz [b], Georges Beaudoin [a,*], Eric C. Grunsky [c], M. Beth McClenaghan [d], Carl Duchesne [b], Emilie Boutroy [e]

[a] Département de Géologie et de Génie Géologique, Université Laval, Quebec, QC G1V0A6, Canada
[b] Département de Génie Chimique, Université Laval, Quebec, QC G1V0A6, Canada
[c] Department of Earth and Environmental Sciences, University of Waterloo, Waterloo, ON, N2L3G1, Canada
[d] Geological Survey of Canada, Ottawa, ON K1A0E8, Canada
[e] Agnico Eagle Mines Limited, Val d'Or, Qc, Canada

ARTICLE INFO

Article history:
Received 3 November 2015
Received in revised form 13 April 2016
Accepted 17 April 2016
Available online 25 April 2016

Keywords:
Magnetite
Trace elements
Indicator mineral exploration
Volcanogenic massive sulfide deposits
Geochemical censored data
Partial least squares discriminant analysis

ABSTRACT

The petrography and mineral chemistry of magnetite from fifteen volcanogenic massive sulfide (VMS) deposits in Canada, and the Lasail VMS deposit in Oman, as well as from two VMS-associated banded iron formations (BIF), Austin Brook (New Brunswick, Canada) and Izok Lake (Nunavut, Canada), were investigated using optical microscopy, electron probe micro-analyzer (EPMA), and laser ablation-inductively coupled plasma-mass spectrometry (LA-ICP-MS). The method of robust estimation for compositional data (robCompositions) was applied to investigate geochemical censored data. Among thirty-seven elements analyzed by EPMA and/or LA-ICP-MS in magnetite from the studied deposits/bedrock lithologies, only the results for Si, Ca, Zr, Al, Mg, Ti, Zn, Co and Ni contain <40% censored values, and thus could be imputed using robCompositions. Imputed censored data were transformed using centered log-ratios to overcome the closure effect on compositional data. Transformed data were classified by partial least squares-discriminant analysis (PLS-DA) to identify different compositional characteristics of magnetite from VMS deposits and BIFs. The integration of petrography and mineral chemistry identifies three types of magnetite in VMS settings: magmatic, hydrothermal, and metamorphic. Magmatic magnetite in VMS deposit host bedrocks is characterized by ilmenite exsolution and may be overprinted by metamorphism. Some VMS deposits contain hydrothermal magnetite, which is intergrown with sulfides, and shows a metamorphic overprint as it is partly replaced by common metamorphic minerals including chlorite, sericite, anthophyllite, and/or actinolite, whereas the majority of the deposits are characterized by metamorphic magnetite formed by replacing pre-existing sulfides and/or silicates, and is intergrown with metamorphic minerals. Among VMS deposits of the Noranda mining district, the West Ansil deposit is characterized by hydrothermal-metamorphic magnetite zoned by inclusion-free cores and Si- and Mg-rich rims. Magnetite from the studied VMS-associated BIFs is also metamorphic in origin. Aluminum, Ti and Zn contents of magnetite can separate BIF from the other mineralized and un-mineralized bedrock lithologies in the studied VMS settings.

PLS-DA shows that variable compositions of magnetite slightly discriminate different studied deposits/bedrock lithologies. The geochemical observations suggest that the variation in magnetite chemistry from different VMS settings might be sourced from differences in: 1) the composition and temperature of parental magmas or hydrothermal fluids, 2) the composition of host bedrocks, 3) the composition of co-forming minerals, and 4) oxygen fugacity. PLS-DA distinguishes magnetite compositions from the studied VMS deposits and BIFs from that of the other ore deposit types including Ni–Cu, porphyry Cu-Mo-Au, iron oxide-copper- gold, iron oxide-apatite, and the Bayan Obo REE-Fe-Nb deposit. Magnetite from the VMS settings on average contains lower concentrations of Si, Zr, Al, Mg, Ti, Zn, Co and Ni relative to that from the other mineral deposit types. PLS-DA of magnetite data from VMS deposits and BIFs of the Bathurst mining camp as well as PLS-DA of magnetite compositions from various mineral deposit types yield discrimination models for application to mineral exploration for VMS deposits using indicator minerals in Quaternary lithified sedimentary rocks.

* Corresponding author at: Département de géologie et de génie géologique, Université Laval, Pavillon Adrien-Pouliot, 1065 avenue de la Medecine, Québec, QC G1V0A6, Canada
E-mail addresses: sh.makvandi@gmail.com (S. Makvandi), massoud.ghasemzadeh-barvarz.1@ulaval.ca (M. Ghasemzadeh-Barvarz), Georges.Beaudoin@ggl.ulaval.ca (G. Beaudoin), egrunsky@gmail.com (E.C. Grunsky), bmcclena@nrcan.gc.ca (M.B. McClenaghan), Carl.Duchesne@gch.ulaval.ca (C. Duchesne), emilie.boutroy@agnicoeagle.com (E. Boutroy).

http://dx.doi.org/10.1016/j.oregeorev.2016.04.014
0169-1368/

1. Introduction

Magnetite is a major to an accessory mineral in various rock types and/or mineral deposits. Magnetite from different geologic settings carries a distinctive chemical signature by incorporating a large number of cations into its inverse spinel structure (e.g., Lindsley, 1976; Wechsler et al., 1984; Bowles et al., 2011; Dupuis and Beaudoin, 2011). The spinel group minerals including magnetite have the general formula XY_2O_4, where X is divalent cations such as Mg, Fe, Ni, Mn, Co and Zn, and Y can be trivalent or tetravalent cations such as Si, Al, Fe and V (Deer et al. 1992; Hu et al., 2014). The composition of minor and trace elements in magnetite is controlled by external factors such as the composition of parent magma/hydrothermal fluids, temperature, pressure, oxygen fugacity, silica activity, cooling rate, and partition coefficients between magnetite and co-forming minerals (Mollo et al., 2013; Dare et al., 2012, 2014). The composition of magnetite as a petrogenetic indicator and/or an exploration tool has been studied using electron probe micro-analysis (EPMA) and laser ablation-inductively- coupled plasma-mass spectrometry (LA-ICP-MS) to measure trace elements with detection limits (DL) typically below the ppm level (Longerich et al., 1996; Dupuis and Beaudoin, 2011; Dare et al., 2012, 2014).

1.1. Magnetite of various origins

Given that the chemistry of magnetite can be affected by physico-chemical conditions at the time of formation, it is expected that magnetite grains formed under similar conditions are characterized by similar compositions, whereas those formed in different geologic environments show different chemical signatures (Dupuis and Beaudoin, 2011; Nadoll et al., 2014). Variable composition of magnetite, which is commonly present as a major to an accessory mineral in both magmatic and hydrothermal ore deposits, can help in discriminating between different mineral deposits or rock types. Dare et al. (2014) studied trace element composition of magnetite from a variety of magmatic and hydrothermal deposits and proposed a multi-element diagram showing the partitioning behavior of trace elements in magnetite during crystallization from magmatic melts or hydrothermal fluids.

In magmatic systems, magnetite can form during fractionation of silicate melts and/or crystallization of sulfide melts. Magnetite crystallized from sulfide melts is commonly enriched in chalcophile elements such as Ni, Cu, and PGE, whereas magnetite grains formed from silicate melts are enriched in lithophile elements such as Cr, Ti, V, Al, Mn, Sc, Nb, Ga, Ge, Ta, Hf, W and Zr (Dare et al., 2012, 2014; Boutroy et al., in press). The concentration of lithophile elements such as V and Cr in magnetite can indicate which stage of fractionation of a silicate melt the magnetite formed in, and if the composition of parental magma was evolved by magma mixing (e.g., Tegner et al., 2006; Dare et al., 2014). Intergrowths of magnetite and ilmenite lamellae are common signatures of magnetite in magmatic systems (Liu et al., 2015). Exsolution of ilmenite from a high-temperature precursor during silicate melt fractionation can also affect the distribution of trace elements in magnetite. Méric (2011) showed that Ti, Hf, Mg, Mn, Nb, Sc, Ta, W and Zr commonly tend to be concentrated in ilmenite rather than in the co-existing magnetite.

Variable composition of hydrothermal magnetite is most likely the result of geological and mineralogical complexity of hydrothermal mineral deposits (Nadoll et al., 2014). Hydrothermal magnetite is commonly enriched in Si and Ca, whereas it is depleted in Ti, Al, Zr, Hf, Nb, Ta, and Sc that are relatively immobile in hydrothermal fluids (e.g., Ray and Webster, 2007; Dupuis and Beaudoin, 2011). Dare et al. (2014) showed that the chemical signature of magnetite formed at high temperatures (~500–700 °C) in magmatic-hydrothermal systems (e.g., porphyry and IOCG deposits) is similar to the chemistry of magnetite crystallized from evolved intermediate magmas. This magnetite is typically enriched in Ni, V, Co, Zn, Mn, and Sn. Dare et al. (2014) showed that co-crystallization of magnetite and Cu-bearing sulfides results in Cu depletion in magnetite as Cu is preferentially incorporated in co-forming sulfides. Makvandi et al. (2016) showed that magnetite from the Izok Lake (Nunavut, Canada) and Halfmile Lake (New Brunswick, Canada) VMS settings may form during regional metamorphism: 1) by replacing pre-existing silicate and/or sulfides, 2) as a result of decomposition of Fe-bearing silicates, or 3) by recrystallization of precursor magnetite. Their observations also suggest that the distribution of trace elements in metamorphic magnetite is mainly controlled by the composition of host rocks, the grade of metamorphism, and oxygen fugacity.

1.2. Mineral exploration and provenance studies using magnetite chemistry

The composition of magnetite from various mineral deposit types has been the focus of several recent studies (e.g., Dupuis and Beaudoin, 2011; Boutroy et al., in press; Dare et al., 2014; Nadoll et al., 2014). Dupuis and Beaudoin (2011) established step-wise discriminant diagrams using the chemistry of magnetite and hematite to classify different mineral deposit types. Liu et al. (2015) used a Ge vs. Ga + Co diagram to classify magnetite from Fe-Ti-(V) oxide ores, Fe-Ti-(P) oxide ores, and Ni–Cu deposits. Berzina (2012) showed that magmatic magnetite in porphyry Cu–Mo deposits contains higher Rh and lower Pt and Pd relative to those in barren host rocks. Huang et al. (2014) found that higher Zn, and lower Al and Mg contents of magnetite separate the Shaquanzi Fe–Cu deposit from the Heifengshan and Shuangfengshan Fe deposits. Chen et al. (2015) indicated that magnetite precipitated from Mo-Sn-rich fluids contains higher Sn and Mo, and lower V and Ni relative to that precipitated from evolved felsic magmas. They suggested that the concentration of these elements in magnetite is mainly controlled by oxygen fugacity.

Boutroy et al. (in press) investigated the composition of magnetite from various Ni-Cu-PGE deposits of different geologic settings and ages. They showed that early forming magnetite crystallized from monosulfide solid solution (MSS) is enriched in lithophile elements (Cr, Ti, V, Al, Sc, Nb, Ga, Ta, Hf and Zr), whereas late forming magnetite crystallized from Cu-rich intermediate solid solution (ISS) is depleted in these elements. Makvandi et al. (2016) used trace element compositions of magnetite to discriminate between the Halfmile Lake and Izok Lake volcanogenic massive sulfide (VMS) deposits and their host rocks. They used principal component analysis (PCA) to classify compositions of detrital magnetite from till (glacial sediment) around and down ice of the deposits. The results for both deposits showed that magnetite grains glacially eroded from VMS mineralization by different ice flow phases formed characteristic dispersal trains down ice from the ore zones.

The main objectives of this study are to 1) extend the studies of Makvandi et al. (2016) on compositions of magnetite from VMS settings, and to 2) introduce partial least squares discriminant analysis (PLS-DA) for classification of magnetite sources in till. Thus, this study compares magnetite compositions from Makvandi et al. (2016; Izok Lake and Halfmile Lake VMS deposits) with data from 14 other VMS deposits of various subtypes using PLS-DA. The results were also compared to the composition of magnetite from some other VMS (Dupuis and Beaudoin, 2011), Ni-Cu-PGE (Dare et al., 2012; Boutroy et al., 2012a, in press), IOCG, IOA and Bayan Obo (Boutroy et al., 2012b), and porphyry deposits (Boutroy, 2013). Projecting data from till into PLS-DA subspaces defined by magnetite compositions in bedrocks identifies the sources of magnetite in till.

2. Sample selection and compositional diversity in selected VMS deposits

A total of forty-nine samples from fifteen VMS deposits in Canada (Fig. 1A) and one from Oman (Fig. 1B) formed during a wide range of geologic ages as well as four samples from two VMS-associated BIFs were studied (Table 1). The studied VMS deposits belong to four

subtypes defined by Franklin et al. (2005): 1) felsic-siliciclastic, 2) mafic, 3) bimodal-mafic, and 4) bimodal-felsic. The felsic-siliciclastic subtype comprises three samples from the massive sulfides from the Brunswick #12 ($n = 1$) and Brunswick #6 ($n = 2$) deposits, and three samples from the Halfmile Lake VMS gossans. Eleven samples from the massive sulfides of the Lasail ($n = 4$), Turgeon ($n = 3$) and Little Bay ($n = 4$) mafic VMS deposits were also studied. The bimodal-mafic subtype consists of fourteen samples from the Lac Dufault ($n = 1$), Horne ($n = 1$), West Ansil ($n = 4$), Normetal ($n = 1$), Bell-Allard ($n = 1$), and Amulet A-Upper and Lower ($n = 6$) VMS deposits, as well as nine samples from the Quemont (diabase; $n = 5$), Poirier (diabase; $n = 1$), and Amulet A-Upper and Lower (dalmatianite; $n = 2$) host bedrocks. Six samples from the bimodal-felsic Izok Lake deposit (Nunavut, Canada), two samples from the silicate facies BIF associated with the Izok Lake deposit, as well as two samples from the oxide and sulfide facies BIFs associated with the Austin Brook VMS deposit are also investigated in this study.

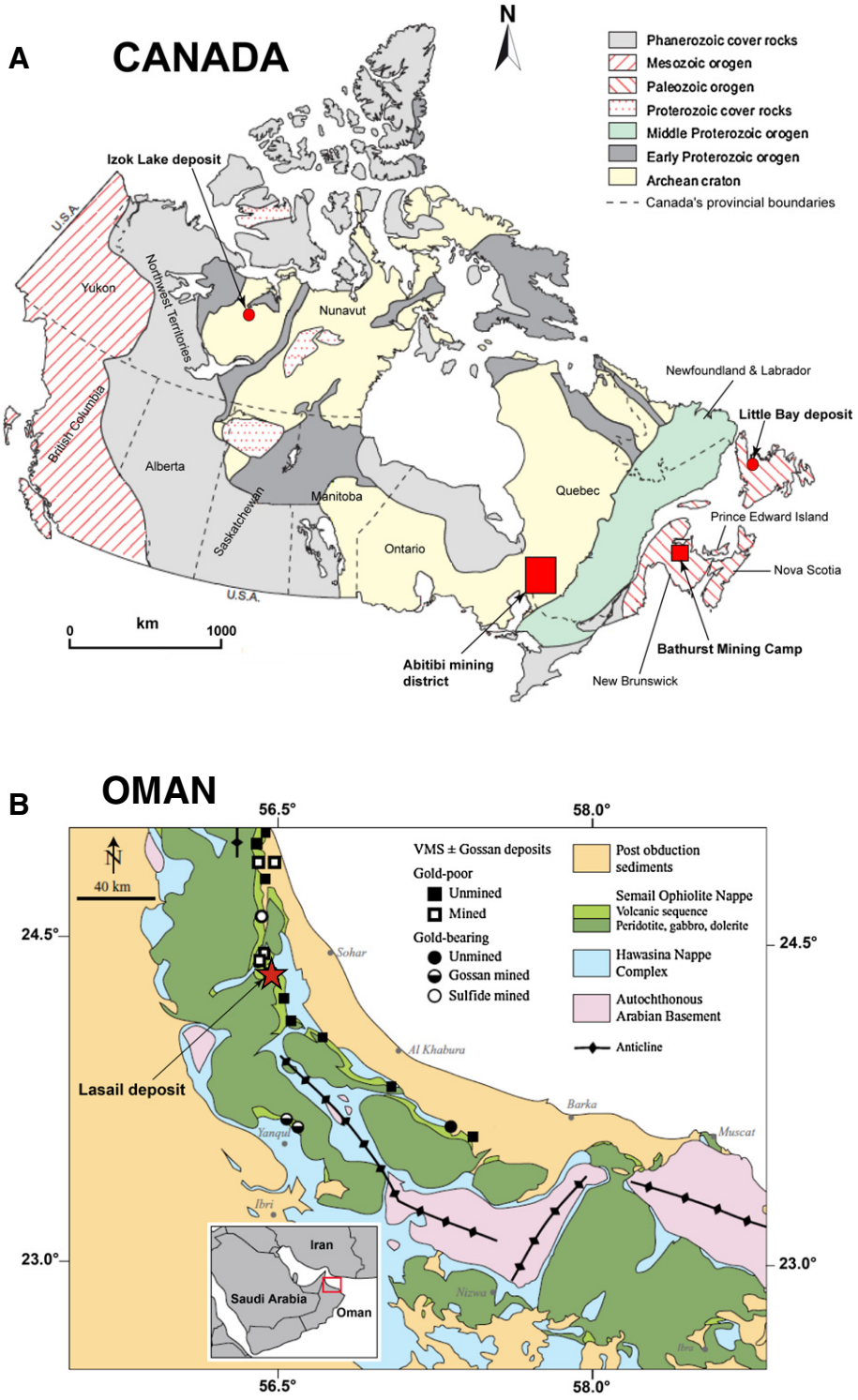

Fig. 1. Locations of studied VMS deposits and VMS-associated BIFs on simplified bedrock geology maps of A) Canada (modified from Galley et al., 2007) and B) Oman (modified from Gilgen et al., 2014). The Bathurst Mining Camp includes: Brunswick #12, Brunswick #6, Halfmile Lake, Turgeon and Austin Brook deposits. The Abitibi mining district includes: Horne, Amulet-A-Upper & Lower, Lac Dufault, Normetal, West Ansil, Bell-Allard, Quemont and Poirier deposits. The Lasail mafic VMS deposit is hosted by the Semail Ophiolite, and located in Oman.

Table 1
List of VMS deposits studied.

Name	Location	District/Camp	Orebody age (Ma)	Orogen	Metamorphic facies	VMS setting	Host rocks composition	Reference source
Austin Brook	Canada, NB	Bathurst	465	Appalachian	Upper greenschist	Felsic-Siliciclastic	Tuffite	Energy, Mines and Resources Canada (1989), Goodfellow and McCutcheon (2003), Franklin et al. (2005)
Brunswick #6	Canada, NB	Bathurst	465	Appalachian	Upper greenschist	Felsic-Siliciclastic	Aphyric to feldspar phyric rhyolite, tuff, crystal tuffite	Goodfellow and McCutcheon (2003), Franklin et al. (2005)
Brunswick #12	Canada, NB	Bathurst	465	Appalachian	Upper greenschist	Felsic-Siliciclastic	Quartz and feldspar-phyric crystal tuff	Goodfellow and McCutcheon (2003), Franklin et al. (2005)
Halfmile Lake	Canada, NB	Bathurst	465	Appalachian	Upper greenschist	Felsic-Siliciclastic	Tuffaceous sandstone and siltstone with minor shale	Goodfellow and McCutcheon (2003), Franklin et al. (2005)
Turgeon	Canada, NB	Bathurst	465	Appalachian	Lower greenschist	Mafic	Basalt	Kettles (1987), Lalonde and Beaudoin (2015)
Little Bay	Canada, NL	Lush's Bight	470	Appalachian	Greenschist	Mafic	Pillow basalt	Swinden and Kean (1988), Evans et al. (1992), Franklin et al. (2005)
Lasail	Oman	Sohar	95	Semail (Tethyan)	Prehnite-pumpellyite facies	Mafic	Pillow basalt	Franklin et al. (2005), Alabaster and Pearce (1985)
Lac Dufault	Canada, QC	Noranda	2700	Abitibi (Kenoran)	Lower greenschist	Bimodal-Mafic	Archean felsic to mafic volcanic rocks	Rivé et al. (1990), Franklin et al. (2005)
Horne	Canada, QC	Noranda	2700	Abitibi (Kenoran)	Lower greenschist	Bimodal-Mafic	Archean felsic to mafic volcanic rocks	Gibson and Watkinson (1990), Franklin et al. (2005)
West Ansil	Canada, QC	Noranda	2698	Abitibi (Kenoran)	Lower greenschist	Bimodal-Mafic	Archean felsic to mafic volcanic rocks	Ministere des Ressources naturelles du Quebec, (1996), Franklin et al. (2005)
Bell-Allard	Canada, QC	Matagami	2720	Abitibi (Kenoran)	Lower greenschist	Bimodal-Mafic	Archean felsic to mafic volcanic rocks	Franklin et al. (2005), Loannou and Spooner (2007)
Normetal	Canada, QC	Noranda	2727	Abitibi (Kenoran)	Lower greenschist	Bimodal-Mafic	Archean felsic to mafic volcanic rocks	Energy, Mines and Resources Canada (1989), Franklin et al. (2005)
Amulet	Canada, QC	Noranda	2698	Abitibi (Kenoran)	Amphibolite	Bimodal-Mafic	Archean felsic to mafic volcanic rocks	Gibson and Kerr (1993), Hall (1982)
Amulet dalmatianite	Canada, QC	Noranda	2698	Abitibi (Kenoran)	Amphibolite	Bimodal-Mafic	Archean felsic to mafic volcanic rocks	Gibson and Kerr (1993), Hall (1982)
Quemont diabase	Canada, QC	Noranda	2700	Abitibi (Kenoran)	Lower greenschist	Bimodal-Mafic	Archean felsic to mafic volcanic rocks	Gibson and Watkinson (1990), Franklin et al. (2005)
Poirier diabase	Canada, QC	Joutel	2730	Abitibi (Kenoran)	Lower greenschist	Bimodal-Mafic	Archean felsic to mafic volcanic rocks	Energy, Mines and Resources Canada (1989), Gibson and Kerr (1993), Franklin et al. (2005)
Izok Lake	Canada, Nu	Slave	2730	Slave (Kenoran)	Amphibolite	Bimodal- Felsic	Dacite	Franklin et al. (2005)
Izok Lake-BIF	Canada, Nu	Slave	2730	Slave (Kenoran)	Amphibolite	Bimodal- Felsic	Basalt	Franklin et al. (2005)

The data from the Izok Lake and Halfmile Lake deposits are from Makvandi et al. (2016).

2.1. Geologic settings

2.1.1. Felsic-siliciclastic VMS deposits and VMS-associated BIF

The felsic-siliciclastic type VMS deposits including the world-class Brunswick #12, Brunswick #6, and Halfmile Lake, as well as the Austin Brook VMS associated BIFs, all are located within the Bathurst mining camp (BMC; New Brunswick, Canada; Fig. 1A). These deposits form part of a Middle Ordovician island-arc and back-arc system developed on the Gondwanan continental margin of the Appalachian orogen (Goodfellow et al., 2003; Lentz and McCutcheon, 2006). All felsic-silisiclastic VMS deposits of the BMC are hosted by the Northern Miramichi Highlands that consists of four different tectonic blocks: Fournier, California Lake, Tetagouche, and Sheephouse Brook (van Staal et al., 2003). The Brunswick #12 and #6 massive sulfide deposits are hosted by the Nepisiguit Falls Formation of the Tetagouche Group (van Staal et al., 1992; Lentz and Goodfellow, 1993). They occur within volcaniclastic mudstones underlain by fine- to coarse-grained, crystal-rich tuffs, porphyritic intrusions and reworked pyroclastic and volcaniclastic rocks of the Nepisiguit Falls Formation (Lentz and Goodfellow, 1996; Lentz and McCutcheon, 2006). The massive sulfides are also overlain by rhyolitic volcanic rocks and associated sedimentary rocks of the Flat Landing Brook Formation (Lentz and Goodfellow, 1993). The Tetagouche Group was metamorphosed to the upper greenschist facies (Lentz and McCutcheon, 2006). Massive sulfides at the Brunswick #12 deposit are mostly associated with carbonate-, silicate-, and chert-facies iron formations, whereas oxide facies iron formations are most prevalent at Austin Brook and Brunswick #6 deposits (McCutcheon et al., 1997). The Austin Brook deposit is principally a magnetite-hematite Algoma-type iron formation, which caps and/or is laterally equivalent to a massive sulfide zone (Peter and Goodfellow, 1996; McCutcheon et al., 1997).

Similar to the Brunswick VMS deposits, the Halfmile Lake deposit is hosted by the Nepisiguit Falls rocks of the Ordovician Tetagouche Group (Adair, 1992; McCutcheon et al., 2000; McCutcheon and Walker, 2001; Mireku and Stanley, 2006). The deposit footwall zone consists of felsic volcanic (quartz ± feldspar-phyric tuffs, cherty tuffs, and aphyric felsic tuffs of rhyolitic and dacitic composition) and epiclastic rocks intruded by quartz-feldspar porphyritic intrusions. The hanging wall comprises predominantly of felsic volcanic rocks and minor epiclastic rocks (Mireku and Stanley, 2006; Budulan et al., 2013, 2015). The Halfmile Lake deposit is capped by a preglacial gossan subcroping over the South Upper AB zone caps (Boyle, 2003), which formed as a result of sulfide oxidation by surficial chemical weathering during late Pliocene to the onset of Pleistocene (1.05–2.3 Ma), prior to Quaternary glaciation. Halfmile Lake gossan is characterized by primary bedrock structures such as banding, folding, and brecciated fault zones that are in sharp contact with the underlying supergene sulfide zone (Boyle, 2003).

2.1.2. Mafic VMS deposits

The Turgeon VMS deposit, located within the BMC (Fig. 1A), is characterized by chlorite-pyrite hydrothermal alteration and massive to brecciated Cu–Zn mineralization (Lalonde and Beaudoin, 2015). The deposit is hosted by the volcano-sedimentary rocks of the Ordovician Fournier Group in the Elmtree-Belledune Inlier (van Staal et al., 1990). The footwall of the Turgeon deposit comprises of basalt and andesite, whereas the hanging wall mainly consists of rhyolite (Lalonde and Beaudoin, 2015). The footwall volcanic rocks of the Turgeon deposit are generally metamorphosed to the lower-greenschist facies (van Staal et al., 1991).

The Little Bay deposit, in the central Mobile Belt (Newfoundland, Canada; Fig. 1A), is hosted by ~505 Ma ophiolitic rocks of the Lushs Bight Group (Kean et al., 1995; Goodfellow et al., 2003). The deposit occurs within Early Ordovician pillow lavas fed by diabase and gabbro

dikes, and minor agglomerate and breccia (Kean et al., 1995; Piercey and Hinchey, 2012). The deposit consists of massive lenses, pods, veins, and sulfide veinlets and sulfide-bearing quartz veins (Piercey and Hinchey, 2012).

The Lasail deposit is in the Semail ophiolite of Oman (Fig. 1B; Alabaster and Pearce, 1985), and hosted by the Geotimes unit consisting of basaltic pillow lavas and rare massive flows, which is overlain by the Lasail unit. The Late Cretaceous Geotimes and Lasail units occurred in ocean spreading ridge and related off-axis volcanic environments, respectively (Gilgen et al., 2014). The Lasail unit comprises basaltic to felsite flows and subvolcanic sheets. Based on the distribution of hydrothermal metamorphic mineral assemblages, Alabaster and Pearce (1985) showed that the Geotimes unit and stockwork zones at the top of the Lasail unit were metamorphosed to the upper greenschist facies, whereas prehnite-pumpellyite facies metamorphism affected the Lasail ore body and its hanging wall.

2.1.3. Bimodal-mafic VMS deposits

All studied bimodal-mafic VMS deposits are located in the Archean Abitibi subprovince (Quebec, Canada; Fig. 1A). The Abitibi subprovince consists of syngenetic VMS and gold-rich VMS deposits, in addition to sulfide-rich, gold-bearing quartz veins, and Cu-Au-bearing sulfide veins, all hosted by felsic volcanic complexes (Gaboury and Pearson, 2008). The Abitibi subprovince comprises volcanosedimentary sequences intruded by plutonic rocks showing evidence of arc formation and evolution, arc-arc collision, and arc fragmentation (Daigneault et al., 2004).

The Noranda camp is situated in the south-central part of the Abitibi subprovince and hosts several VMS deposits including West Ansil, Lac Dufault, Horne, Normetal, Quemont, and Amulet A-Upper and Lower (Amulet). The Noranda volcanic complex was intruded by the synvolcanic Flavrian and Powell plutons (Kennedy, 1985; Galley et al., 2000). The Archean volcanic succession in the Noranda camp was metamorphosed to the prehnite-pumpellyite or the lower greenschist facies (Dimroth et al., 1983; Monecke et al., 2008), though the intrusion of the Lac Dufault granodiorite caused contact metamorphism up to the amphibolite facies in the Amulet deposit area (Hall, 1982). The Poirier VMS deposit is located in the southern part of the Harricanna-Turgeon Belt, in the northern part of the Abitibi subprovince (Jacob and Tremblay, 2012).

The Bell-Allard deposit is in the Matagami mining camp, which is situated in the northern part of the Abitibi subprovince (Mortensen, 1993; Ross et al., 2014). The Matagami camp contains >60 Mt of zinc-rich ore (Ross et al., 2014). The Bell-Allard deposit is located at the contact between the rhyolitic unit of the Watson Lake Group (Ross et al., 2014), and the Wabassee Group andesitic lavas (Ross et al., 2014; Genna et al., 2014). The Poirier deposit is hosted by the Joutel Volcanic Complex (northern Abitibi subprovince) composed of rhyolitic volcaniclastites, rhyolites, basalts, andesite and sediments (Jacob and Tremblay, 2012).

2.1.4. Bimodal-felsic VMS deposit and VMS-associated BIF

The Izok Lake bimodal-felsic VMS deposit is located in the northern part of the Archean Slave Structural Province (Nunavut, Canada; Fig. 1A), and is hosted within 2.7–2.67 Ga granite greenstone terrain of folded, faulted, and metamorphosed rocks of the Point Lake Formation, Yellowknife Supergroup (Morrison, 2004; Bleeker and Hall, 2007). In the Izok Lake area, the Point Lake Formation consists of felsic to mafic metavolcanic and metasedimentary rocks, and was intruded by 2.68 and 2.58 Ga syn-volcanic to post-volcanic granitic plutons, and by the Helikian Mackenzie gabbro dike swarm (Bleeker et al., 1999). The hydrothermal alteration zone associated with the Izok Lake deposit consists mainly of a Mg-enrichment zone that contains the assemblage chlorite-biotite-cordierite in close proximity to the massive sulfides (McClenaghan et al., 2015). The stringer zone at the Izok Lake deposit is gahnite-rich, and is in close association with the Mg-enrichment. Silicate facies iron formation also occurs in association with the Izok Lake deposit overlying the upper contacts of dacite and basalt flows (Morrison, 2004). Rocks in the Izok Lake area were metamorphosed to the amphibolite facies (Thomas, 1978; Morrison, 2004).

3. Methodology

3.1. Sample preparation

Polished thin sections were made of mineralized an/or unmineralized bedrock samples collected from the selected VMS deposits. For the Izok Lake and Halfmile Lake samples only, polished mounts containing about 50 mineral aggregates and/or grains from the 0.25–2.0 mm ferromagnetic heavy mineral concentrates were also prepared for each sample (Makvandi et al., 2016). In general, three to five magnetite grains per section, and up to 25 grains per mount were selected for chemical analysis by EPMA (Table 1). The number of analyses was based on 1) distribution of magnetite in a PTS or mount, 2) textural relationships between magnetite and other minerals (inclusion or intergrowth), and 3) the diversity of mineral associations. Magnetite grains larger than 100 μm, with surfaces free of inclusions were also analyzed by LA-ICP-MS. In total, 368 magnetite grains from the studied VMS deposits, bedrocks, and associated BIFs were analyzed by EPMA, from which 133 grains were also analyzed by LA-ICP-MS (Table 1).

3.2. Analytical methods

3.2.1. EPMA

Following the methodologies of Dupuis and Beaudoin (2011) and Boutroy et al. (in press), thirteen elements including K, Ca, Al, Si, Ti, Mg, Mn, Cr, V, Sn, Cu, Zn, and Ni, which their average concentration in magnetite is commonly above their minimum detection limit were analyzed using a CAMECA SX-100 EPMA at Université Laval (Québec, Canada). The device is equipped with five wavelength-dispersive spectrometers. Following the methods described by Makvandi et al. (2016), analyses were conducted using a 15 kV accelerating voltage with 100 nA beam current, and 10 μm beam size. Under high current conditions a wide beam diameter is needed to prevent heating of magnetite. Background was measured on both sides of the peak for 15 to 20 s at an offset position in a flat region, where the spectrum is experimentally verified to be free of interfering element X-ray wavelengths. Depending on the element, concentrations were counted over the peak for 20 to 60 s (Dupuis and Beaudoin, 2011; Boutroy et al., in press). Simple oxides (GEO Standard Block of P and H Developments) and/or natural minerals (Mineral Standard Mount MINM 25–53, Astimex Scientific) were used to calibrate the instrument (Jarosewich et al., 1980; Dupuis and Beaudoin, 2011). The range of detection limits for EMPA data is shown in Appendix-I A.

3.2.2. LA-ICP-MS

Analyses were carried out at Université du Québec à Chicoutimi (UQAC) using a Resonetics Resolution M-50 Excimer 193 nm laser coupled with an Agilent 7700× ICP-MS. Analyses used a speed stage of 3 μm/s, a laser frequency of 10 Hz, and a power of 5 mJ per pulse. GSE-1G, a single Fe-rich reference material containing all the required elements was used for calibration, and Fe as determined by EPMA, was used as an internal standard (Savard et al., 2012). Depending on the grain size of magnetite, 20 and 43 μm beam sizes were used to ablate linear trenches across the grains in order to determine their average compositions, especially for those characterized with exsolution textures or growth zoning. The quality of analyses was also monitored with reference materials GSD-1G and BC-28 (a natural magnetite from the Bushveld Complex). Data reduction was performed using the software Iolite. Following Dare et al. (2012), the distribution of ^{24}Mg, ^{25}Mg, ^{27}Al, ^{29}Si, ^{34}S, ^{44}Ca, ^{45}Sc, ^{47}Ti, ^{49}Ti, ^{51}V, ^{52}Cr, ^{53}Cr, ^{55}Mn, ^{57}Fe, ^{59}Co, ^{60}Ni, ^{65}Cu, ^{66}Zn, ^{69}Ga, ^{71}Ga, ^{74}Ge, ^{89}Y, ^{90}Zr, ^{92}Zr, ^{93}Nb, ^{95}Mo,

^{101}Ru, ^{105}Pd, ^{107}Ag, ^{111}Cd, ^{115}In, ^{118}Sn, ^{121}Sb, ^{178}Hf, ^{181}Ta, ^{182}W, ^{187}Re, ^{193}Ir, ^{195}Pt, ^{197}Au, ^{208}Pb and ^{209}Bi in magnetite were measured by LA-ICP-MS. Contents of S, Si, Ca, Mn, Mg, Al and Ti were used to monitor the data to ensure that the measured signals were free of inclusions. Following the methods described by Dare et al. (2012, 2014) and Boutroy et al. (in press), the content of Si and Ca of magnetite was taken from the EPMA results. The range of detection limits for LA-ICP-MS data is shown in Appendix-I B.

3.3. Statistical methods

3.3.1. Pre-treatment of compositional data

Censored geochemical data contain values below detection limits (DL) for one or several elements in a sample (Helsel, 2005). Different methods have been proposed to carry statistical analysis of censored data. Excluding censored data, or arbitrary substitutions are commonly used, however, they are not recommended because they introduce biased estimates of summary statistics (Helsel, 2005; Beaudoin and Dupuis, 2009). Thus, following Makvandi et al. (2016) methodology, EPMA and/or LA-ICP-MS results including up to 40% censored data were transformed using the robCompositions *R*-package. In this technique, the k-nearest neighbors (impKNNa) function is used to impute censored values using the Aitchison distance (Filzmoser et al., 2009; Hron et al., 2010; Bacon-Shone, 2011; Grunsky et al., 2013). The imputation is performed based on the median of corresponding data of the k-nearest un-censored neighbors where k is ≥1. Calculating the error between the randomly imputed and the original values determines the k value. The optimal k yields the smallest error. Imputed values are often greater than the lower DL, however, they never exceed 3 times the DL, and are always within the range of low precision (Grunsky et al., 2013).

Closure of compositional data arises from use of concentration variables with a constant sum (Aitchison, 1986; Whitten, 1995; Grunsky, 2010). Compositional data only carry relative information; hence, the concentration is given by the ratios between components. Imputed censored data were transformed using centered-log ratio (clr; Makvandi et al., 2016), which is a symmetric transformation with an orthonormal basis (Egozcue et al., 2003), appropriate for multivariate statistical techniques such as PLS-DA.

3.3.2. Partial least squares discriminant analysis

Makvandi et al. (2016) used PCA to distinguish magnetite compositions between VMS deposits and host bedrocks from the Izok Lake and Halfmile Lake VMS deposits. Principal component analysis is a clustering method looking for maximum variations in the data that may cause sample classification (Wishart, 2013). However, as mentioned previously, this study aims to classify different VMS deposits/bedrock lithologies based on magnetite compositions. This makes the data amenable to the application of robust classification methods such as partial least squares discriminant analysis (PLS-DA), which is a supervised classification technique using labeled data (Wishart, 2013). It sharpens the separation between groups of observations by rotating PCA components, which results in the maximum separation among classes, and the identification of the variables responsible for the separation of different classes (de Iorio et al., 2008). Appendix-II shows the results of investigating a dataset of magnetite compositions from the studied VMS settings using both multivariate statistical techniques, PCA and PLS-DA. Comparing the results of both methods indicates that PLS-DA enhances the separation between different samples.

PLS-DA consists of a classical PLS regression to model the response matrix (**Y**) by means of a predictive matrix (**X**) (Wold et al., 2001). When the traditional multiple linear regression (MLR) is not applicable due to highly correlated structure of data, PLS is an alternative. PLS-DA is a regression where the **Y** matrix is a set of binary variables (0 and 1) - describing the categories of observations (Wold et al., 2001). Discriminant analysis determines which variables discriminate between two or more naturally occurring classes. PLS-DA allows the discrimination of different observations based on their attributes, and is a standard tool in chemometrics because of its ability to deal with multicollinearity (Barker and Rayens, 2003; Westerhuis et al., 2008).

In the PLS method, the objective is to extract a set of orthogonal components, so-called latent variables, to relate the **X** (N × K) and **Y** (N × M) matrices by maximizing the covariance between them using the following bilinear decompositions (Wold et al., 2001; Eriksson et al., 2001):

$$\mathbf{X} = \mathbf{TP}^{\mathbf{T}} + \mathbf{E} \tag{1}$$

$$\mathbf{Y} = \mathbf{TQ}^{\mathbf{T}} + \mathbf{F} \tag{2}$$

$$\mathbf{T} = \mathbf{XW}* \tag{3}$$

where **T** (N × r), containing r orthogonal PLS components (scores), represents the common latent variable space of both **X** and **Y**. For Eqs. (1)–(3), **P** (N × r) and **Q** (M × r) are the loadings matrices for **X** and **Y**, respectively; and **W***, the so-called the weight matrix, consists of the coefficients of the linear combinations of the **X** variables that are the most predictive of **Y** (i.e. linear combinations of element compositions that are the most discriminative of the deposit samples). **E** and **F** in these equations are the model residuals for **X** and **Y** matrices, respectively.

To interpret the PLS model, one can use the scores scatter plot in which the projection of observation in the latent variable space is shown. In this plot, the observations are grouped by similar attributes such as chemical composition. However to determine the variables (i.e. elements) responsible for the classification, **w***__q__ loadings biplot must be generated. In this biplot the weights **w*** and loadings **q** are shown simultaneously to interpret: a) the importance of **X**-variables, b) the correlation between **X**-variables, and c) the relationship between **X**-variables and **Y**-variables (classes). Variables located at the extreme corners of the plot contribute most to the scores plot separation, whereas those located near the origin plot have less impact in the model. In addition, the **X**-variables, which are grouped together in the same quadrants have positive correlation and provide the same information, whereas the variables located on opposite quadrants are negatively correlated (Eriksson et al., 2001). The **X** and **Y** variables having similar coordinates are also positively correlated whereas those positioned on opposite quadrant have negative correlations.

Variable contributions are metrics that can be used to diagnose the causes for shifts from one cluster to another one in a latent variable space or from the origin of the score scatter plot (Miller et al., 1998). In this study, compositional variable contributions were calculated using Eq. (4) to characterize the mean composition of each sample group, and to identify differences in average distribution of trace elements in magnetite between samples in latent variable space:

$$C_k = (X_a - X_b)\sqrt{\sum_i \left(\frac{t_a - t_b}{s_{ti}}\right)^2 w_{Ki}^2} \tag{4}$$

where C_k is the score contribution of variable k, X and **t** are the original variables and score values of sample (a), here the origin of score plot, and sample (b) respectively, **w** is the weighting value for variable **k**, and **s** corresponds to the standard deviation of score vector i. The mean composition of a sample group can be discriminated by positive/negative contributions of chemical elements indicating higher/lower concentrations of elements relative to the average of the dataset.

A parameter summarizing the importance of each **X**-variable on the class discrimination is the variable importance on the projection (VIP; Chong and Jun, 2005) defined as:

$$VIP_k = \sqrt{\frac{K\sum_{a=1}^{r}\left(\left(\frac{w_{ak}}{\|w_a\|}\right)^2 (q_a^2 t'_a t_a)\right)}{\sum_{a=1}^{r}(q_a^2 t'_a t_a)}} \tag{5}$$

where K is the total number of **X**-variables, w_{ak} is the weight of kth variable in the ath principal component, r is the number of principal component, and $\mathbf{w_a}$, $\mathbf{t_a}$ and $\mathbf{q_a}$ are the ath column vector of **W** and **T** and **Q**, respectively. The VIP is a weighted sum of squares of the PLS weights in which the amount of explained **Y**-variance in each dimension is taken into account (Eriksson et al., 2001). According to Eriksson et al. (2001), variables with VIP larger than 1 are most influential in the model (classification) because the average of the squared VIPs is equal to 1. Variables having a VIP between 0.8 and 1.0 represent moderately influential variables, whereas a VIP value of <0.8 is less important.

Considering that the variables (concentration) have different scales (e.g., ppm, wt%), prior to PLS-DA, data were auto-scaled to give all variables an equal opportunity to contribute to the model (Geladi and Grahn, 1996). Auto-scaling is implemented by applying variance scaling on a mean-centered dataset (Geladi and Grahn, 1996; Kramer, 1998). Variance scaling is obtained by dividing each value of a variable by the standard deviation of that variable (Geladi and Grahn, 1996).

4. Results

4.1. Petrography of magnetite in different VMS deposits and associated BIFs

Fig. 2 shows typical textures of different magnetite types in VMS deposits, bedrocks and BIFs. In samples examined in this study, hydrothermal magnetite from the Horne (Fig. 2A), Normetal, Turgeon (Fig. 2B), and Little Bay deposits are intergrown with chalcopyrite, pyrite, sphalerite and/or pyrrhotite. This magnetite was partly replaced by the assemblage chlorite ± calcite ± siderite (Fig. 2A and B). In the Turgeon deposit, hematite was partly replaced by magnetite (Fig. 2B). In contrast to magnetite from these deposits, magnetite from the Lac Dufault (Fig. 1C), Amulet A-Upper and Lower (Amulet), Bell-Allard (Fig. 2D), Lasail, Brunswick #12, Brunswick #6 (Fig. 2E), and Izok Lake (Fig. 2F) deposits formed by replacing sulfides (commonly chalcopyrite, pyrite and/or sphalerite). In the Bell-Allard deposit, magnetite contains galena and quartz inclusions, and partly replaced altaite (PbTe) and tellurantimony (Sb_2Te_3), which occur in veinlets (Fig. 2D). Galena and quartz fill the interstices between magnetite grains. The Brunswick #6 (Fig. 2E) and Brunswick #12 deposits contain euhedral magnetite with galena inclusions, which is in equilibrium with the assemblage chlorite-quartz. Magnetite that replaced sulfides from all VMS deposits, other than the Amulet and Izok Lake deposits, are intergrown with the assemblage chlorite ± sericite ± quartz ± calcite ± epidote (Fig. 2C, D and E). In the Amulet deposit, magnetite is intergrown with chlorite, sericite, calcite, quartz, anthophyllite and biotite, whereas in the Izok Lake deposit, magnetite is commonly intergrwon with actinolite (Fig. 2F). At Izok Lake, magnetite contains sphalerite and chalcopyrite inclusions, and is characterized by magnesioferrite exsolution (Fig. 2F).

The West Ansil deposit is characterized by massive magnetite, and the open spaces between magnetite grains are commonly filled by quartz and chlorite, and lesser with chalcopyrite and pyrrhotite (Fig. 2G). Remobilized chalcopyrite commonly veins massive magnetite (Fig. 2G; Boucher, 2011). Magnetite in the West Ansil deposit also shows growth zoning commonly consisting of rhombic shaped cores of pure magnetite rimmed by Si (average: 1.5 wt.%)- and Mg (average: 0.1 wt.%)-rich magnetite with sulfide and silicate inclusions (Fig. 3A-C).

In the Izok Lake deposit silicate facies BIF, anhedral, fine-grained magnetite partly replaced biotite-hornblende intergrowths (Fig. 2H), whereas in the Austin Brook oxide- and sulfide-facies BIF, magnetite is sub- to euhedral, medium grained, and commonly coarser than coexisting minerals, such as hematite and/or pyrite and pyrrhotite (Fig. 2I and J). Hematite is widespread in association with magnetite-bearing Austin-oxide facies BIF-mag, and occurs as hematite-rich bands (Fig. 2I). The Austin Brook oxide-facies BIF is generally devoid of sulfides. In contrast, fine-grained pyrite and pyrrhotite are commonly associated with Austin Brook sulfide facies BIF-mag (Fig. 2J). In both Austin Brook BIFs, magnetite is surrounded by the assemblage chlorite ± siderite ± sericite (Fig. 2I and J).

In the studied VMS deposits, magmatic magnetite that is mainly characterized by ilmenite exsolution (Fig. 2K and L) occurs in Amulet dalmatianite (Fig. 2K), and diabasic host bedrocks of the Quemont (Fig. 2L), Poirier and Horne deposits. As shown by Makvandi et al. (2016), the Halfmile Lake gossans also consist of magmatic magnetite, since they formed at least in part by weathering of bedrock syenite. Magmatic magnetite from the Amulet dalmatianite is mainly associated with chlorite, sericite, anthophyllite, and biotite (Fig. 2K), whereas that from the Quemont (Fig. 2L) and Poirier diabasic bedrocks was replaced by and/or spatially associated with the assemblage chlorite + calcite + epidote + quartz. Magmatic magnetite characterizing host bedrocks of the Horne deposit was largely altered by the assemblage chlorite and quartz and so it could not be analyzed by LA-ICP-MS.

4.2. Geochemistry of magnetite from various VMS settings

Among the elements determined by EPMA and LA-ICP-MS, the data contain <40% censored values only for Si, Ca, Zr, Al, Mn, Mg, Ti, Zn, Co, and Ni. Table 2 presents the mean compositions of magnetite from the studied VMS deposits and BIFs. The whole dataset of raw EPMA (n = 371) and LA-ICP-MS (n = 133) data is also in Appendix-III. To distinguish magnetite compositions in VMS settings, the LA-ICP-MS magnetite analyses were investigated by PLS-DA (Fig. 4). The biplot of the first and second PLS-DA components ($\mathbf{qw^*_1}$-$\mathbf{qw^*_2}$, Fig. 4A) illustrates correlations among elemental variables and deposit classes. For instance, there is positive correlation among Si, Ca and Mg, and between Ti and Al (Fig. 4A). Correlations among elements control the distribution of magnetite analyses in PLS-DA first and second scores ($\mathbf{t_1}$-$\mathbf{t_2}$; Fig. 4B). Magmatic magnetite from the Halfmile Lake gossans, Amulet dalmatianite, and diabasic host bedrocks of the Quemont and Poirier deposits plot in the right side of $\mathbf{t_1}$-$\mathbf{t_2}$ (Fig. 4B) mainly because of their high Ti values ($\mathbf{qw^*_1}$-$\mathbf{qw^*_2}$; Fig. 4A). Higher Zr, Ti and Ni, and lower Si, Ca, Al and Mg values than the average of the dataset allow Quemont magmatic

Fig. 2. A selection of figures showing mineral aggregates from VMS deposits and VMS-associated BIFs studied. A) Magnetite from the Horne bimodal-mafic VMS deposit in association with chalcopyrite, pyrite, pyrrhotite, and chlorite. B) Magnetite from the Turgeon mafic VMS deposit partly replaced by hematite. Turgeon magnetite is commonly associated to chalcopyrite, siderite, chlorite and calcite. C) Back-scattered electron image of a mineral aggregate from the Lac Dufault bimodal-mafic VMS deposit composed of magnetite, pyrite, sphalerite, chalcopyrite, chlorite, sericite and quartz. D) Magnetite from the Bell-Allard bimodal-mafic VMS deposit with inclusions of altaite and tellurantimony. Galena and quartz fill interstices between magnetite grains. E) Mineral aggregate from the Brunswick #6 felsic-siliciclastic VMS deposit including disseminated magnetite with galena inclusions, and in association with chlorite and quartz. F) Magnetite from the Izok Lake bimodal-felsic VMS deposit is intergrown with actinolite, and contains sphalerite and chalcopyrite inclusions. This magnetite is also characterized by magnesioferrite exsolution. Pyrite is molded in magnetite. G) Quartz, chlorite, chalcopyrite and pyrrhotite fill the open spaces between magnetite grains from the West Ansil bimodal-mafic VMS deposit. H) Mineral aggregate from the Izok Lake banded iron formation (BIF) composed of magnetite intergrown with biotite and hornblende. I) Mineral aggregate from the Austin Brook oxide facies BIF composed of euhedral magnetite associated to widespread occurrence of hematite. Siderite and chlorite are present as inclusions in magnetite, and also slightly replace magnetite from edges. J) Mineral aggregate from the Austin Brook sulfide facies BIF composed of euhedral magnetite associated to chlorite and sericite, and to lesser extends, with pyrite and pyrrhotite. K) Euhedral magnetite from dalmatianite host bedrocks of the Amulet A-Upper & Lower (Amulet) bimodal-mafic VMS deposit textured with ilmenite lamellae, and in association with anthophyllite, sericite, chlorite and biotite. L) Mineral aggregate from diabasic host bedrocks of the Quemont deposit composed of altered magnetite with ilmenite exsolutions, in association with calcite, epidote, chlorite, and quartz. Abbreviations: magnetite- Mag; chalcopyrite- Ccp; pyrite- Py; pyrrhotite- Po; chlorite- chl; hematite- Hem; siderite- Sd; calcite- Cal; sphalerite- Sp; sericite- Ser; quartz- Qz; altaite- Alt; tellurantimony- Tel; galena- Gn; actinolite act; magnesioferrite- Mfr; biotite- Bi; hornblende- Hbl; anthophyllite- Ath; epidote- Ep.

magnetite to form a distinct cluster, in Fig. 4B. Halfmile Lake magnetite also makes an overlapping cluster because of higher amounts of Al, Ti and Ni, and lower Si, Zr and Mg. In contrast to magmatic magnetite, high Si, Ca and Mg, and low Ti and Ni contents (Fig. 4A) isolate zoned magnetite from the West Ansil deposit in the left side of Fig. 4B. Hydrothermal magnetite from the other VMS deposits and BIFs plot in between magmatic magnetite and the West Ansil magnetite in $\mathbf{t_1}$-$\mathbf{t_2}$ (Fig. 4B). The $\mathbf{qw^*_1}$-$\mathbf{qw^*_2}$ loading values display a different chemical signature for Austin-oxide facies and Austin-sulfide facies BIF-mag that causes their separation in $\mathbf{t_1}$-$\mathbf{t_2}$ space, whereas Austin-sulfide facies and Izok-silicate facies BIF-mag share similar chemistry (Fig. 4A) clustering in the vicinity of each other in Fig. 4B. Austin-oxide facies BIF-mag forms a cluster in the high $\mathbf{t_2}$ region in Fig. 4B mainly because of high Zn and Co, and low Al and Ti contents (Fig. 4A), whereas Izok-silicate facies BIF-mag forms an overlapping cluster in the high $\mathbf{t_1}$, low $\mathbf{t_2}$ region mainly because of high values of Ti and Al. Magnetite from the Turgeon and Little Bay mafic VMS deposits also plot as overlapping clusters in the low $\mathbf{t_1}$ and $\mathbf{t_2}$ region (Fig. 4B). Fig. 4A suggests that the distribution of magnetite analyses from the Izok Lake bimodal-felsic and Amulet bimodal-mafic deposits in Fig. 4B is mainly controlled by high

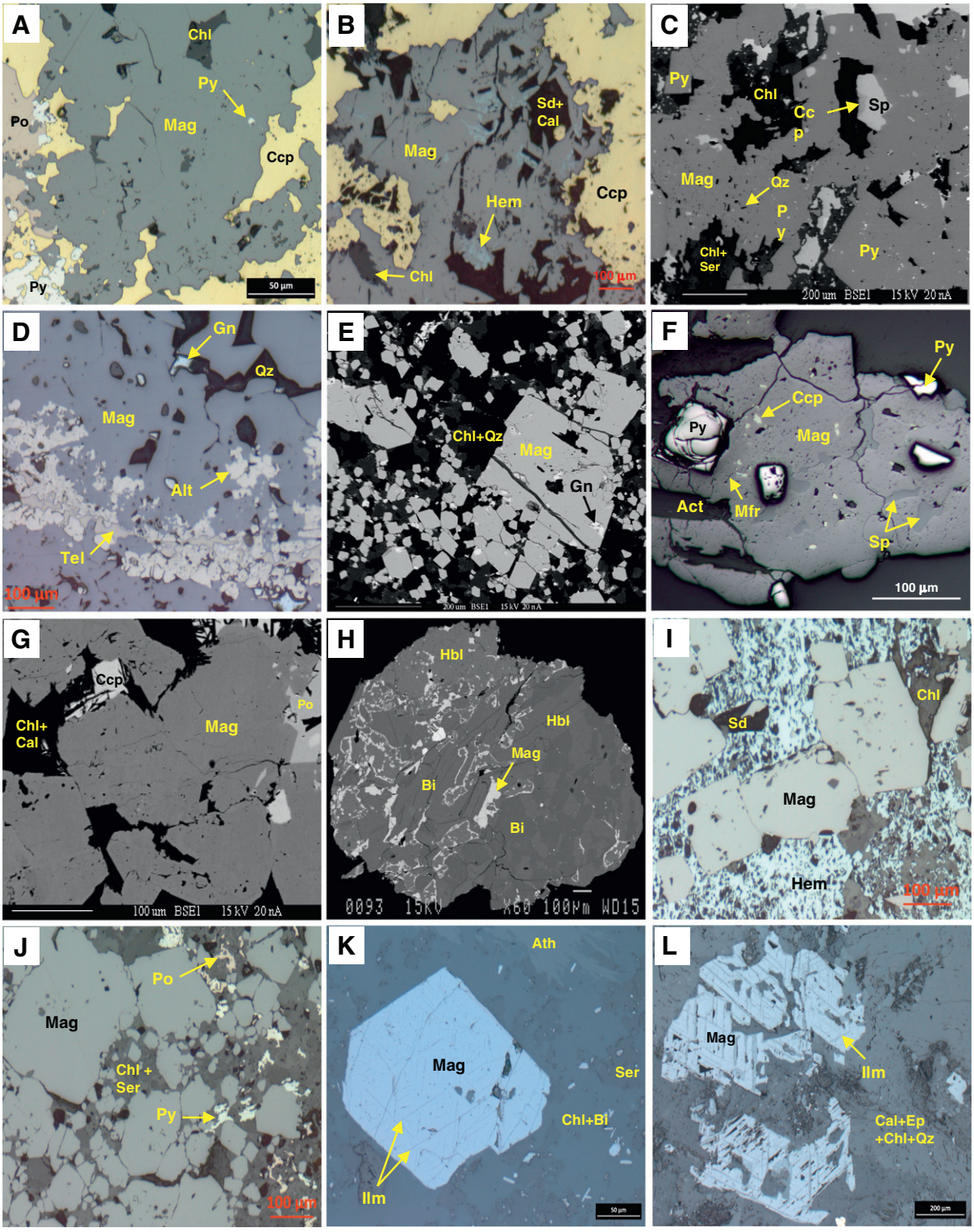

Zn, and low Ti and Al values. Although different types of magnetite from the majority of VMS deposits and BIFs are scattered in $\mathbf{t_1}$-$\mathbf{t_2}$ space, the variable contributions presented in Appendix-IV show that the mean composition of each deposit cluster is discriminated by distinct chemical signatures. For instance, the mean composition of the Lac Dufault deposit is mainly isolated by the positive contribution of Si and Zn, and the negative contribution of Ti and Ni, whereas that of the Horne cluster is discriminated by negative contributions of Al, Mn, Ti and Zn, and positive contributions of Ca, Zr and Mg (Fig. 4A-C; Appendix-IV H and I).

The VIP plot shows that Ti is an important factor separating the composition of magnetite in all deposits other than Horne in Fig. 4B, whereas Mn is not useful in this classification. Aluminum is also important in classifying all magnetite groups other than West Ansil, Normetal, and Amulet dalmatianite (Fig. 4C). Silicon, Mg and Ni are moderate to important variables in the discrimination of magmatic magnetite (Fig. 4C). Calcium is also a significant variable in separation of magmatic magnetite from all VMS deposits other than that of the Halfmile Lake gossans. In separation of BIF-mag, Ti, Al, Zn are important factors, whereas Si, Ca and Mg are not useful (Fig. 4C). The geochemical characteristics of magnetite from the studied VMS deposits, host bedrocks and VMS-associated BIFs are summarized in Table 3.

4.3. PLS-DA of magnetite compositions of the BMC VMS deposits and BIFs

PLS-DA is used to distinguish magnetite compositions of VMS deposits and VMS-associated BIFs in the BMC (Fig. 5). The $\mathbf{qw^*_1}$-$\mathbf{qw^*_2}$ biplot shows that higher Ti, Al, Ni and Co, and lower Si, Ca, Zr, Mn and Mg (Fig. 5A) separate the Halfmile Lake magmatic magnetite from hydrothermal magnetite from the other VMS deposits and BIFs in $\mathbf{t_1}$-$\mathbf{t_2}$ space (Fig. 5B). The VIP plot (Fig. 5C) also indicates the importance of all elements other than Mn in this classification. Fig. 5A and B show that the variable composition of hydrothermal magnetite results in discrimination of different BMC deposits in $\mathbf{t_1}$-$\mathbf{t_2}$. For instance, magnetite from the Turgeon mafic VMS deposit is discriminated by high Si, Ca and Mg, and low Ni and Zn. Magnetite from the Brunswick #12 and Brunswick #6 felsic-siliciclastic subtype VMS deposits form overlapping clusters in Fig. 5B. Fig. 5C shows that Si, Zr, Al, Mn and Ti are main contributors separating magnetite from these felsic-siliciclastic VMS deposits from that of the other deposits in $\mathbf{t_1}$-$\mathbf{t_2}$. In contrast to magnetite from the Brunswick #12 and Brunswick #6 deposits, BIF-mag from Austin-oxide facies and Austin-oxide facies show distinctive chemistry (Fig. 5A) that separates them in $\mathbf{t_1}$-$\mathbf{t_2}$ space (Fig. 5B). The VIP plot displays that Zr, Al and Ti are the main variables discriminating Austin-oxide facies BIF-mag, whereas Ca, Mg, Co and Ni are important in the classification of Austin-sulfide BIF (Fig. 5C).

To investigate the potential of PLS-DA models in the classification of magnetite compositions in unconsolidated sediments in the BMC, the LA-ICP-MS data of magnetite in till samples from the Halfmile Lake deposit area (Makvandi et al., 2016) are projected into the $\mathbf{t_1}$-$\mathbf{t_2}$ space defined by different studied BMC deposits (Fig. 5B). As illustrated in Fig. 5D, a high proportion of Halfmile Lake till magnetite grains plot in the field for magnetite from the Halfmile Lake deposit.

4.4. PLS-DA of magnetite composition from the studied VMS settings and that from previous studies

4.4.1. Magnetite from different VMS deposit subtypes

There is a lack of LA-ICP-MS data for magnetite from VMS deposits in the literature. Therefore, in order to distinguish trace element compositions of magnetite from VMS deposits, a dataset consisting of EPMA data of 484 magnetite grains from the selected VMS deposits and those investigated by Dupuis and Beaudoin (2011) was evaluated using PLS-DA (Fig. 6). Fig. 6 discriminates various VMS deposits based on Si, Al, Mn, and Mg compositions of magnetite, since the other elements analyzed by EPMA (V, Cr, Zn, Cu, Ni, K, Sn, Ca, and Ti) contain >40% censored values. Given that Fig. 6A-C study the chemical signatures of magnetite in VMS mineralized bedrocks, the data corresponding to magmatic magnetite and BIF-mag are not considered in the corresponding PLS-DA analysis. The $\mathbf{qw^*_1}$-$\mathbf{qw^*_2}$ biplot (Fig. 6A) shows a positive correlation between Mn and Mg located in the same quadrant, and a negative correlation between Si and Al plotting in opposite quadrants. The loadings indicate that Mn and Si discriminate different samples along the first PLS-DA component ($\mathbf{qw^*_1}$), whereas Al and Mg are the main contributors to classify VMS deposits along the second component direction ($\mathbf{qw^*_2}$). Lower Si values isolate the majority of bimodal-felsic VMS deposit samples in the right side of $\mathbf{t_1}$-$\mathbf{t_2}$ (Fig. 6A and B). A high proportion of Izok Lake magnetite grains project in the high $\mathbf{t_1}$ and low $\mathbf{t_2}$ region (Fig. 6B) due to relatively high concentrations of Mn and Mg, and low Si and Al contents (Fig. 6A). The $\mathbf{qw^*_1}$-$\mathbf{qw^*_2}$ biplot shows that magnetite from the Kudz Ze Kayah (Yukon, Canada), Normetal, Ducktown (Tennessee, USA), and Boliden (Skelleftea area, Sweden) deposits are mainly characterized by high Al values, whereas high Si values characterizes magnetite from the Caribou (New Brunswick, Canada), ODP Mound (Middle Valley, Pacific Ocean), Bell-Allard, and Brunswick #12 deposits (Fig. 6A). In contrast to the majority of VMS deposit samples scattered in $\mathbf{t_1}$-$\mathbf{t_2}$ score plot, GP4F (Yukon, Canada) magnetite cluster in the high $\mathbf{t_1}$ and $\mathbf{t_2}$ values (Fig. 6B) mostly because of its relatively high Al and Mn, and low Si and Mg contents (Fig. 6A). The variable contributions presented in Appendix-V show that despite forming overlapping clusters in $\mathbf{t_1}$-$\mathbf{t_2}$ space, the mean composition of magnetite from each VMS deposit could be isolated by distinct chemical signatures.

The VIP plot shows the importance of Si, Al, Mn and Mg in the classification of different VMS deposits and indicates that Mn is a moderate to important variable in separating all deposits other than Horne (Fig. 6C). It also shows that Al and Mg are important in separating magnetite from all bimodal-mafic VMS deposits in $\mathbf{t_1}$-$\mathbf{t_2}$ space other than that of the West Ansil and Amulet deposits, whereas Si is the only discriminant for magnetite from these two deposits. Fig. 6A indicates that magnetite from the West Ansil deposit is characterized by high Si and low Mn, whereas high Mn and low Si values isolate magnetite from the Amulet deposit. In addition to Mn, Al and Mg are also discriminant for all bimodal-felsic deposits, whereas Si is only important in classification of the Izok Lake, Boliden and GP4F (Fig. 6C).

4.4.2. Magnetite from various mineral deposit types

The previous results demonstrated how magnetite compositions can be used to discriminate between different VMS deposits, BIFs, and VMS hosting bedrocks within a geologic setting and/or from various geologic environments. Fig. 7 shows the results for PLS-DA of data from this study compared with the composition of magnetite from Ni–Cu, porphyry, IOCG and IOA deposit types as well as that from the Bayan Obo deposit (Dare et al., 2012, 2014; Boutroy, 2013; Boutroy et al., 2012a,b, in press). Censored values from the literature were imputed for Si, Ca, Al, Mn, Mg, Ti, Zn, Co and Ni. As shown by Makvandi et al. (2016) and from results of this study, Si and Ca are important variables in the classification of magnetite from VMS deposits, such that only studies that report Si and Ca are used in the comparison.

PLS-DA loadings in the first component show positive correlations among all elements in $\mathbf{qw^*_1}$ separating the porphyry, IOCG, IOA, and Bayan Obo deposits from the Ni–Cu, VMS and BIF deposit types (Fig. 7A). Magnetite from Ni–Cu deposits forms a cluster with small overlap with that of VMS deposits and BIFs in Fig. 7B. Magnetite from Ni–Cu deposits contains higher Ni values and lower values of all other trace elements relative to the average of the dataset. Compared with the other deposit types, magnetite from VMS and BIF deposit types show more chemical similarity (Fig. 7A) because they cluster close to each other in $\mathbf{t_1}$-$\mathbf{t_2}$ space (Fig. 7B). VMS and BIF magnetite contain low concentration of all trace elements other than Ca relative to the average of the dataset. Magmatic magnetite from the Quemont and Poirier diabasic bedrocks plots in the field for Ni–Cu deposits (Fig. 7B). In contrast to Ni–Cu and VMS samples, magnetite from porphyry, IOCG, IOA, and the Bayan Obo deposits overlap in $\mathbf{t_1}$-$\mathbf{t_2}$ space (Fig. 7B). However, the

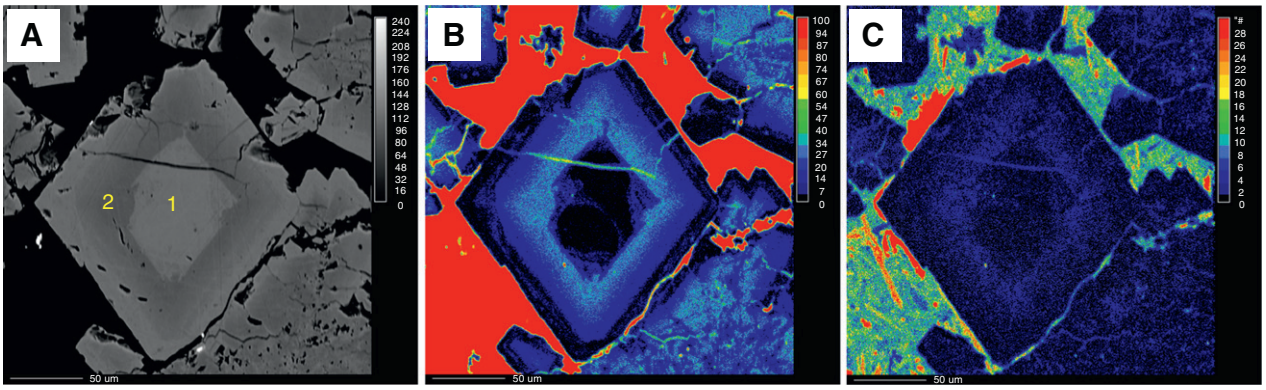

Fig. 3. Chemical maps of zoned magnetite from the West Ansil bimodal-mafic VMS deposit by electron microprobe (beam size 3 μm). A) Back-scatter image shows growth zoning in euhedral magnetite with a bright core of pure magnetite (1) rimmed/replaced by B) Si- and C) Mg-rich magnetite (2).

variable contributions presented in Appendix-VI indicate that the mean composition of each deposit type is distinguished by small differences in the level of elements enrichment. In comparison, the mean composition of the Bayan Obo cluster indicates higher Ca and Zn values relative to that of the other deposit clusters. Higher Ni, Ti and Co values discriminates the IOA group mean composition. Magnetite from IOCG deposits are characterized by higher Si, Al and Mn and lower Ti and Ni relative to that of IOA deposits. High Al and Zn values isolate the mean composition of the porphyry deposits cluster. The VIP values (Fig. 7C) confirm moderate to important impacts of Si, Al, Mn, Ti and Co in classification of all mineral deposit types other than VMS and BIF. Calcium and Zn also contribute moderately to significantly to separation of magnetite groups. Magnesium is a moderately important factor in discrimination of porphyry and IOCG deposits, whereas Ni is discriminant for all groups other than porphyry and IOCG (Fig. 7C).

To study the potential of PLS-DA models in classification of magnetite in unconsolidated sediments, the data for till magnetite from the Izok Lake and Halfmile Lake VMS areas (Makvandi et al., 2016) are

Table 2
Mean compositions of magnetite (in ppm) from the studied VMS deposits and BIFs. LA-ICP-MS data are used for all elements other than Si and Ca, which include EPMA data.

Sample name	Number of Mag analyses			Si	Ca	Zr	Al	Mn	Mg	Ti	Zn	Co	Ni
	EPMA	LA-ICP-MS											
Austin Brook-oxide BIF	6	5	*Average*	206	116	4	105	2155	82	1	697	32	37
			Std	195	49	4	31	150	36	0.7	48	10	6
Austin Brook-sulfide BIF	7	7	*Average*	1891	162	4	229	1590	203	275	54	0.2	23
			Std	2706	117.2	5	98	435	211	22	17	0.04	39
Brunswick #12	4	4	*Average*	4773	1206	4	101	746	135	61	434	12	8
			Std	535	353	3	48	28	49	23	242	0.3	1
Brunswick #6	7	4	*Average*	1133	111	3	95	772	27	84	117	5	12
			Std	940	49	3	8	28	4	11	28	2	8
Halfmile Lake	15	13	*Average*	70	80	0.3	2014	1449	168	1290	423	43	51
			Std	30	49	0.5	3699	1902	422	3463	853	14	71
Turgeon	14	7	*Average*	837	5899	0.6	442	776	837	95	30	24	0.4
			Std	663	3949	1.2	147	132	663	55	16	30	0.2
Little Bay	14	7	*Average*	6451	191	0.4	750	570	408	267	23	14	4
			Std	3882	176	0.3	785	31	546	84	25	2	0.7
Lasail	12	6	*Average*	1007	6595	3	2838	2631	1282	250	2868	50	153
			Std	358	2049	2	1323	607	333	299	4675	33	100
West Ansil	28	10	*Average*	13,983	505	0.1	261	699	914	17	22	15	1
			Std	3780	398	0.2	430	68	235	44	17	6	1
Bell-Alard	12	10	*Average*	2169	308	0.7	131	784	762	169	21	358	7
			Std	2018	219	0.9	99	134	784	11	16	1104	8
Lac Dufault	6	5	*Average*	3233	314	3	330	1311	207	6	122	20	3
			Std	2268	320	6	260	1210	203	6	84	16	4
Amulet	10	9	*Average*	1499	246	4	1682	1094	2931	725	689	133	28
			Std	2721	422	9	3477	966	6371	1423	1105	289	38
Horne	7	7	*Average*	1889	518	76	948	519	626	619	29	38	16
			Std	4167	381	130	2060	795	609	1265	26	36	22
Normetal	4	2	*Average*	80	82	2	836	58	32	332	1862	8	3
			Std	287	66	1.2	42	2	22	114	2599	1	0.1
Amulet dalmatianite	20	7	*Average*	333	84	6	3041	694	1673	3991	764	19	30
			Std	335	59	14	2593	866	1031	4224	1101	20	35
Poirier diabase	6	4	*Average*	1507	1043	3	2119	225	169	8498	165	39	550
			Std	1237	1310	5	4067	350	211	16,874	320	13	263
Quemont diabase	16	5	*Average*	250	496	12	899	1168	543	28,024	71	53	301
			Std	88	457	7	859	1040	365	12,243	28	7	25
Izok Lake	79	10	*Average*	1264	321	0.5	50	1383	3962	4	331	492	76
			Std	2354	323	0.5	47	1095	4667	3	475	1014	75
Izok Lake-BIF	104	11	*Average*	956	421	0.6	751	659	738	1299	14	1	100
			Std	1301	806	0.3	253	136	1023	693	5	0.4	174

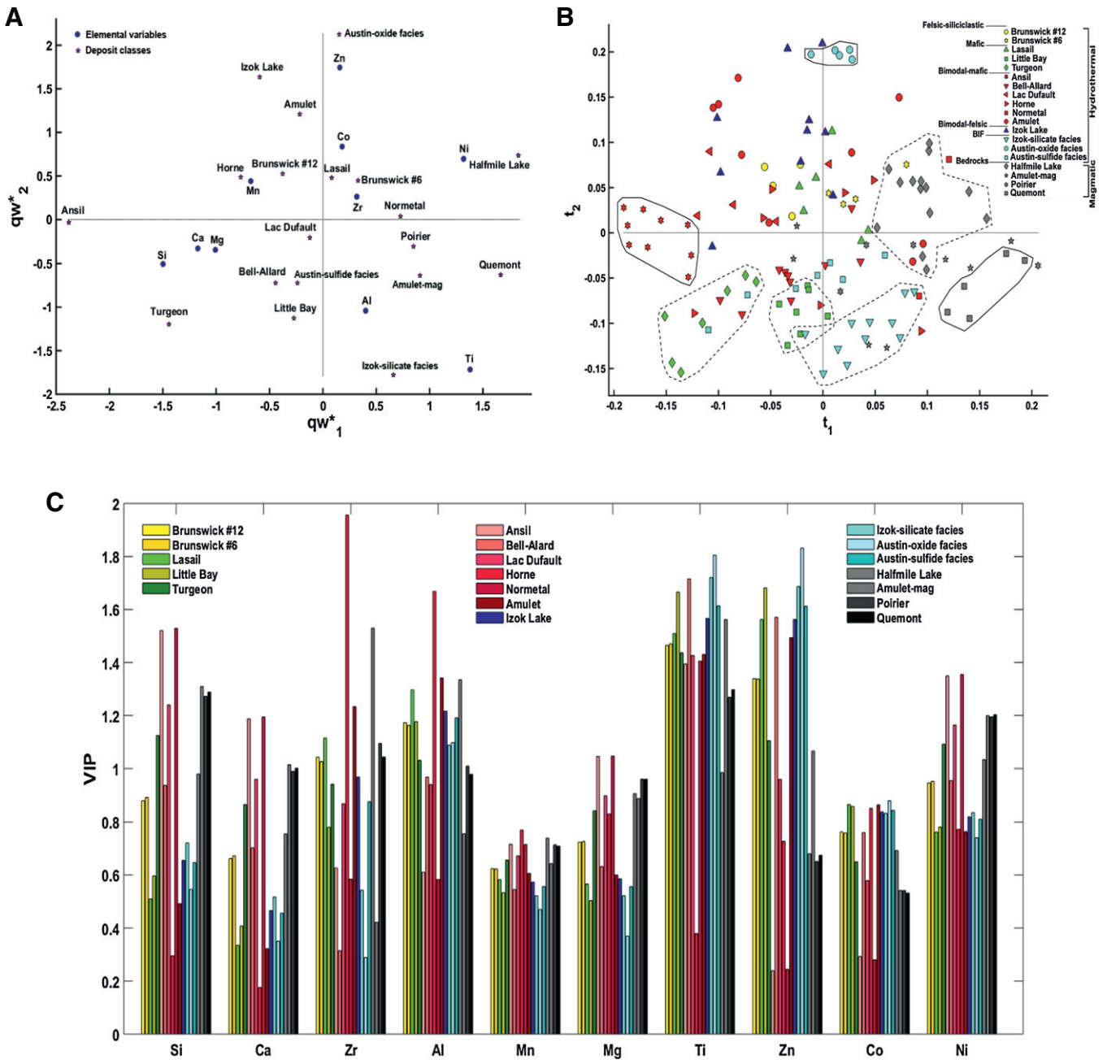

Fig. 4. Partial least squares discriminant analysis (PLS-DA) of Laser Ablation Inductively Coupled Plasma Mass Spectrometry (LA-ICP-MS) data for magnetite from various subtypes of VMS deposits, their host bedrocks, and VMS-associated BIFs. A) The $\mathbf{qw^*_1\text{-}qw^*_2}$ (first and second loadings) plot shows correlations among elemental variables and deposit classes. **B)** The $\mathbf{t_1\text{-}t_2}$ (first and second scores) plot shows the distribution of magnetite analyses from different deposits in the latent variable space defined by $\mathbf{qw^*_1\text{-}qw^*_2}$. The polygons built by solid lines in **B** limit the fields for samples forming distinct clusters, whereas overlapping clusters are limited by dashed lines. **C)** The VIP showing the importance of compositional variables in classification of samples in **B**. Deposits and bedrock lithologies are numbered in **C** to facilitate searching corresponding VIP values.

projected into the $\mathbf{t_1\text{-}t_2}$ space defined by different deposit types (Fig. 7B). As illustrated in Fig. 7D, the majority of till magnetite grains from both areas plot in the field for VMS deposits and associated BIFs.

5. Discussion

Investigation of magnetite compositions from the studied VMS settings allowed us to identify: 1) different types of magnetite associated with mineralization, alteration, and deposit bedrocks; 2) the distribution of trace elements in magnetite from these geologic settings, and 3) discriminator elements, which can be used to classify magnetite from different deposit types and/or bedrock lithologies. Makvandi et al. (2016) identified three types of magnetite in the Izok Lake and Halfmile Lake VMS settings: magmatic, hydrothermal and metamorphic. They suggested that the chemistry of various types of magnetite is controlled by 1) the composition of magmatic/hydrothermal fluids, 2) the composition of co-forming minerals, 3) temperature, 4) the grade of metamorphism, and 5) oxygen and sulfur fugacities. Makvandi et al. (2016) showed that magmatic magnetite is commonly rich in Ti, whereas high Si, Ca and Mg are indicative of hydrothermal magnetite. In contrast, metamorphic magnetite is characterized by variable distribution of trace elements. They demonstrated that Si, Ca, Zr,

Table 3
The geochemical characteristics of magnetite from the studied VMS deposits, host bedrocks and VMS-associated BIFs.

Deposit/bedrock name	Sample type	Magnetite type	Mineral assemblages	Magnetite petrographic features	Discriminant chemical signatures of magnetite*
Austin Brook	Oxide facies iron formation	Metamorphic	Hemtite ± pyrite ± pyrrhotite + chlorite ± siderite	Euhderal to subhedral; fine- to medium-grained; slight hematite replacement	High Zn & Co, low Al & Ti
Austin Brook	Sulfide facies iron formation	Metamorphic	Pyrite + pyrrhotite + chlorite ± sericite	Euhderal to subhedral; fine- to medium-grained	High Zr, Al, Ti & Zn, low Co & Ni
Brunswick #6	Massive sulfide	Metamorphic	Chlorite + quartz + galena	Disseminated; euhderal to subhedral; medium-grained	High Si, Zr, Ti, Zn & Ni, low Al
Brunswick #12	Massive sulfide	Metamorphic	Chlorite + quartz + galena	Disseminated; euhderal to subhedral; fine- to medium-grained	High Si, Zr & Zn, low Al, Ti & Ni
Halfmile Lake	Massive sulfide gossans	Magmatic	Chlorite + quartz + muscovite ± beudantite ± chromite ± cassiterite ± pyrite ± galena ± ilmenite ± rutile ± zircon	Euhedral, fine- to medium-grained; ilmenite or ulvöspinel exsolution; slight chlorite replacement from edges or fractures	High Al, Ti & Ni, low Si, Zr & Mg
Izok Lake	Massive sulfide	Metamorphic	Sphalerite + chalcopyrite + pyrite + actinolite	Euhedral to anhedral; fine- to coarse-grained; magnesioferrite exsolution	High Zn & Ni, low Zr, Al, Ti & Co
Izok Lake BIF	Silicate facies iron formation	Metamorphic	Biotite + hornblende ± almandine ± actinolite	Anhedral; fine-grained	High Al, Ti & Ni, low Zn & Co
Turgeon	Massive sulfide	Hydrothermal	Chalcopyrite + pyrite ± pyrrhotite + chlorite ± calcite ± siderite	Subhedral to anhedral; medium-grained; hematite alteration; metamorphic-hydrothermal minerals replacement	High Si, Ca, Al, Mg, Ti, low Zr, Zn, Ni
Little Bay	Massive sulfide	Hydrothermal	Chalcopyrite + pyrite ± sphalerite ± pyrrhotite + chlorite + quartz	Disseminated, subhedral to anhedral; fine-grained; partly replaced by the assemblage chlorite + quartz	High Al, Ti & Co, low Zn
Lasail	Massive sulfide	Metamorphic	Chalcopyrite + pyrite ± pyrrhotite + chert	Disseminated; anhedral; fine-grained	High Al & Zn, low Zr, Ti & Co
Lac Dufault	Massive sulfide	Metamorphic	Pyrite + sphalerite + chalcopyrite + chlorite + quartz + sericite	Anhedral, fine-grained	High Si, Ca, Zr, Al & Zn, low Mg, Ti & Ni
Horne	Massive sulfide	Hydrothermal	Pyrrhotite + chalcopyrite + sphalerite + pyrite + sericite + chlorite + quartz	Subhedral to anhedral; fine- to medium-grained; partly replaced by the assemblage chlorite + sericite + quartz	High Zr, Mg & Co, low Al
Bell-Allard	Massive sulfide	Metamorphic	Galena + quartz + altaite + tellurantimony	Subhedral to anhedral; fine- to medium-grained	High Si, low Al, Zn & Ni
Normetal	Massive sulfide	Hydrothermal	Chalcopyrite + sphalerite + pyrite + chlorite + sericite	Subhedral to anhedral; fine-grained; partly replaced by the assemblage chlorite + sericite	High Ti, low Si, Ca, Mg & Ni
Amulet	Massive sulfide	Metamorphic	Chalcopyrite + pyrite + sphalerite + sericite + chlorite + anthophyllite	Subhedral to anhedral; fine-grained	High Zr, Zn & Co, low Al & Ti
West Ansil	Massive sulfide	Hydrothermal-metamorphic	Quartz, chlorite, chalcopyrite, pyrrhotite	Massive; euhedral to subhedral; fine- to medium-grained; growth zoning of Si-Mg-poor and Si-Mg-rich magnetite	High Si, Ca & Mg, low Ti & Ni
Amulet dalmatianite	Dalmatianite	Magmatic	chlorite + sericite ± calcite + quartz + anthophyllite + biotite	Euhedral; medium to coarse-grained; Ilmenite exsolution	High Mg, Ti & Zn, low Si, Ca & Ni
Quemont diabase	Diabase	Magmatic	Pyroxene + chlorite + quartz + chalcopyrite ± calcite ± epidote	Coarse-grained; ilmenite exsolution; altered hydrothermal-metamorphic minerals	High Zr, Ti & Ni, low Si, Ca, Al & Mg
Poirier diabase	Diabase	Magmatic	Chlorite + sericite + quartz + Chalcopyrite ± calcite ± epidote	Euhedral; medium-grained; ilmenite exsolution; replaced by hydrothermal-metamorphic minerals from edges and fractures	High Si, Ca, Ti & Ni, low Zr, Al & Mg

* Note that listed chemical signatures were determined based on the results of PLS-DA of transformed (see data pretreatment methodology) compositional data of magnetite. Discriminant elements for classification of magnetite from each deposit/bedrock lithology contain VIP values ≥0.8. High/low indicates the value of an element of interest in magnetite is higher/lower than the average value of that element in the dataset used in Fig. 4.

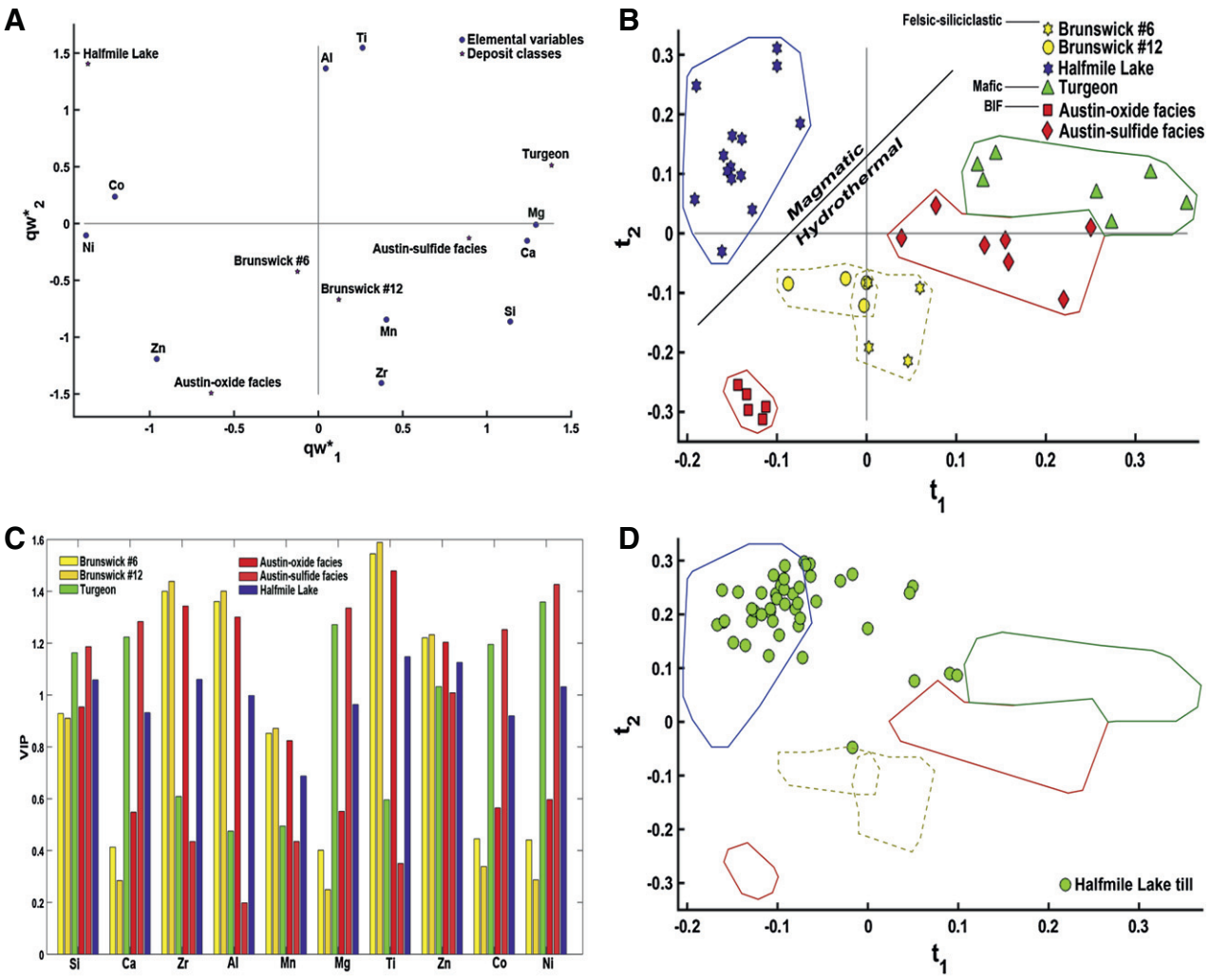

Fig. 5. PLS-DA of LA-ICP-MS data for magnetite from the studied VMS deposits and VMS-associated BIFs of the Bathurst Mining Camp (BMC). **A)** The $\mathbf{qw^*_1}$-$\mathbf{qw^*_2}$ (first and second loadings) plot shows correlations among elemental variables and deposit classes. **B)** The $\mathbf{t_1}$-$\mathbf{t_2}$ (first and second scores) plot shows the distribution of magnetite analyses from different VMS deposits in the latent variable space defined by $\mathbf{qw^*_1}$-$\mathbf{qw^*_2}$. The polygons built by colourful solid lines in **B** limit the fields for samples forming distinct clusters, whereas dashed lines limit the overlapping fields for the Brunswick #6 and Brunswick #12 deposits. C) The VIP showing the importance of compositional variables in classification of samples in B. Deposits and bedrock lithologies are numbered in C to facilitate searching corresponding VIP values. D) Projection of the compositional data of detrital magnetite grains from the Haflmile Lake and area into B.

Al, Ga, Mn, Mg, Ti, Zn, Co, Ni and Cr contents of magnetite is useful in discrimination of magnetite in VMS mineralization from that of their host rocks at Izok Lake and Halfmile Lake.

5.1. Different types of magnetite associated to VMS deposits

5.1.1. Hydrothermal and metamorphic magnetite in massive sulfides

Complexity in geology and mineralogy of hydrothermal ore deposits results in variable composition of hydrothermal magnetite (Nadoll et al., 2014). In the Horne (Fig. 2A), Normetal, Turgeon (Fig. 2B) and Little Bay deposits, magnetite is intergrown with sulfides and is partly replaced by the assemblage chlorite ± sericite ± quartz ± calcite ± siderite (Table 3). This suggests that magnetite co-crystallized with sulfides, and their crystallization, at least in part, predated metamorphism. The Mn, Co and Ti enrichment characterizing magnetite from the Horne deposit (Table 2) may reflect the composition of magmatic-derived, high-temperature (~ 500–700 °C) parental fluids (Nielsen et al., 1994; Toplis and Carroll, 1995; McIntire, 1963; Nadoll et al., 2012, 2014). In addition, the variable composition of Horne magnetite that results in scattering the samples in PLS-DA score space (Fig. 4B) might be a sign of multiple stages of hydrothermal alteration, metamorphism, and/or secondary weathering processes affecting the bedrocks at the time of magnetite growth (Nadoll et al., 2014). In the Turgeon deposit, replacement of hydrothermal magnetite by hematite (Fig. 2B) suggests an increase in the grade of metamorphism and/or oxygen fugacity (Frost, 1979; Klein, 2005). Turgeon magnetite is enriched in Ca (0.6 wt.%; Table 2), consistent with precipitation from low-temperature hydrothermal fluids as well as the mafic composition of the host bedrocks (e.g., Agranier et al., 2007; Dare et al., 2014).

The abundance of silicate and sulfide inclusions in magnetite, and irregular boundaries of magnetite with mineral associations in the Lac Dufault (Fig. 2C), Bell-Allard (Fig. 2D), Brunswick #12, Brunswick #6

Fig. 6. PLS-DA of Electron Probe Micro-Analyzer (EPMA) data for magnetite from various subtypes of VMS deposits investigated in this study and that from Dupuis and Beaudoin (2011). The data for magnetite from the VMS host bedrocks and BIFs are not considered in this analysis. **A)** $\mathbf{qw^*_1}$-$\mathbf{qw^*_2}$ (first and second loadings) shows correlations among elemental variables and deposit classes. **B)** The $\mathbf{t_1}$-$\mathbf{t_2}$ (first and second scores) plot shows the distribution of magnetite analyses from different VMS deposits in the latent variable space defined by $\mathbf{qw^*_1}$-$\mathbf{qw^*_2}$. The polygon built by solid lines in **B** limits the field for magnetite from the GP4F bimodal-felsic VMS deposit. **C)** The VIP showing the importance of compositional variables in classification of samples in **B**. Deposits and bedrock lithologies are numbered in **C** to facilitate searching corresponding VIP values.

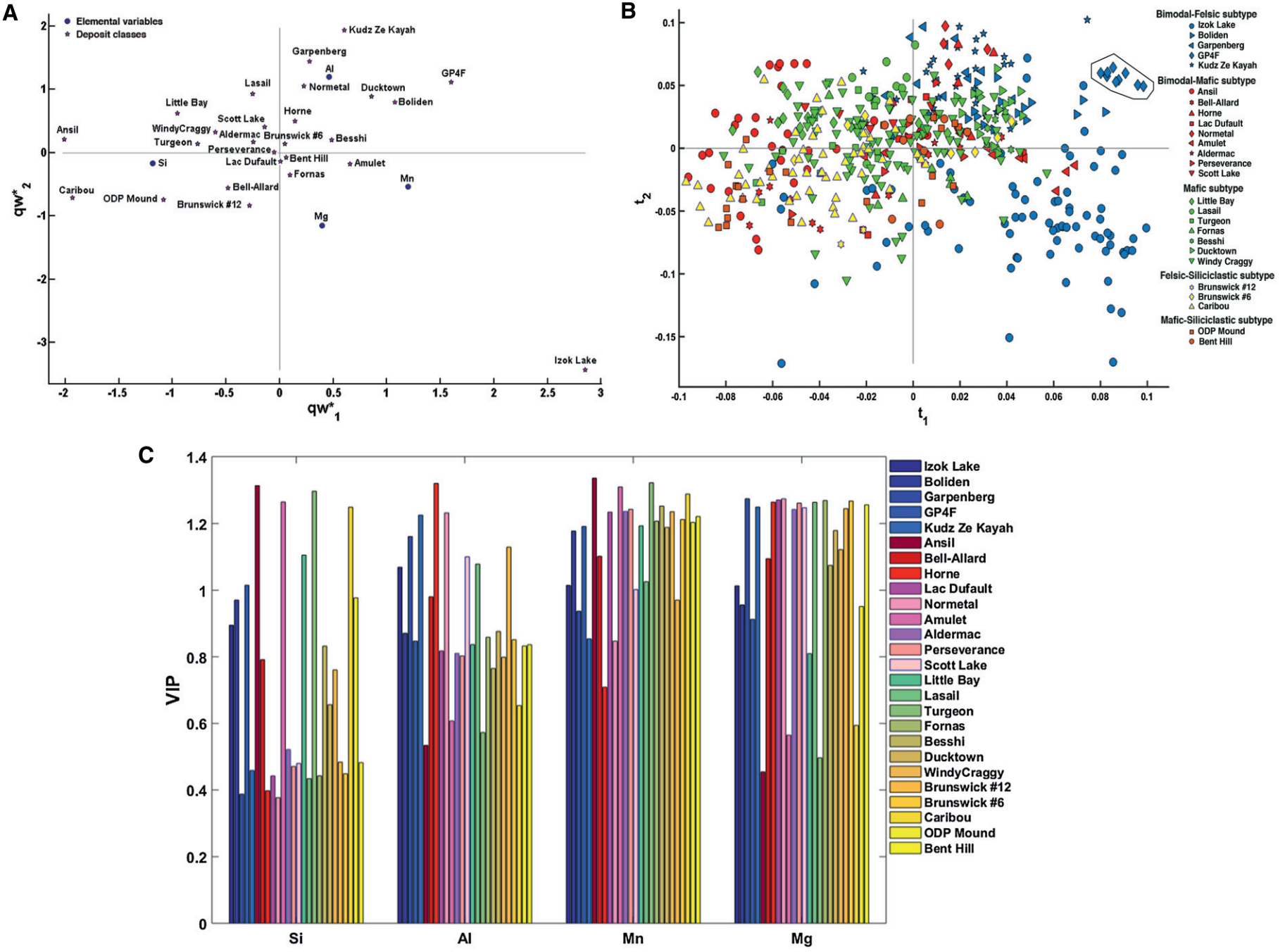
A
Elemental variables
Deposit classes
Kudz Ze Kayah
Garpenberg
Al
GP4F
Lasail
Normetal
Ducktown
Boliden
Little Bay
Horne
Scott Lake
Ansil
WindyCraggy
Aldermac
Brunswick #6
Besshi
Turgeon
Perseverance
Si
Lac Dufault
Bent Hill
Amulet
Fornas
Mn
Caribou
ODP Mound
Bell-Allard
Brunswick #12
Mg
Izok Lake
qw*2
qw*1
B
Bimodal-Felsic subtype
Izok Lake
Boliden
Garpenberg
GP4F
Kudz Ze Kayah
Bimodal-Mafic subtype
Ansil
Bell-Allard
Horne
Lac Dufault
Normetal
Amulet
Aldermac
Perseverance
Scott Lake
Mafic subtype
Little Bay
Lasail
Turgeon
Fornas
Besshi
Ducktown
Windy Craggy
Felsic-Siliciclastic subtype
Brunswick #12
Brunswick #6
Caribou
Mafic-Siliciclastic subtype
ODP Mound
Bent Hill
t2
t1
C
VIP
Si
Al
Mn
Mg
Izok Lake
Boliden
Garpenberg
GP4F
Kudz Ze Kayah
Ansil
Bell-Allard
Horne
Lac Dufault
Normetal
Amulet
Aldermac
Perseverance
Scott Lake
Little Bay
Lasail
Turgeon
Fornas
Besshi
Ducktown
WindyCraggy
Brunswick #12
Brunswick #6
Caribou
ODP Mound
Bent Hill

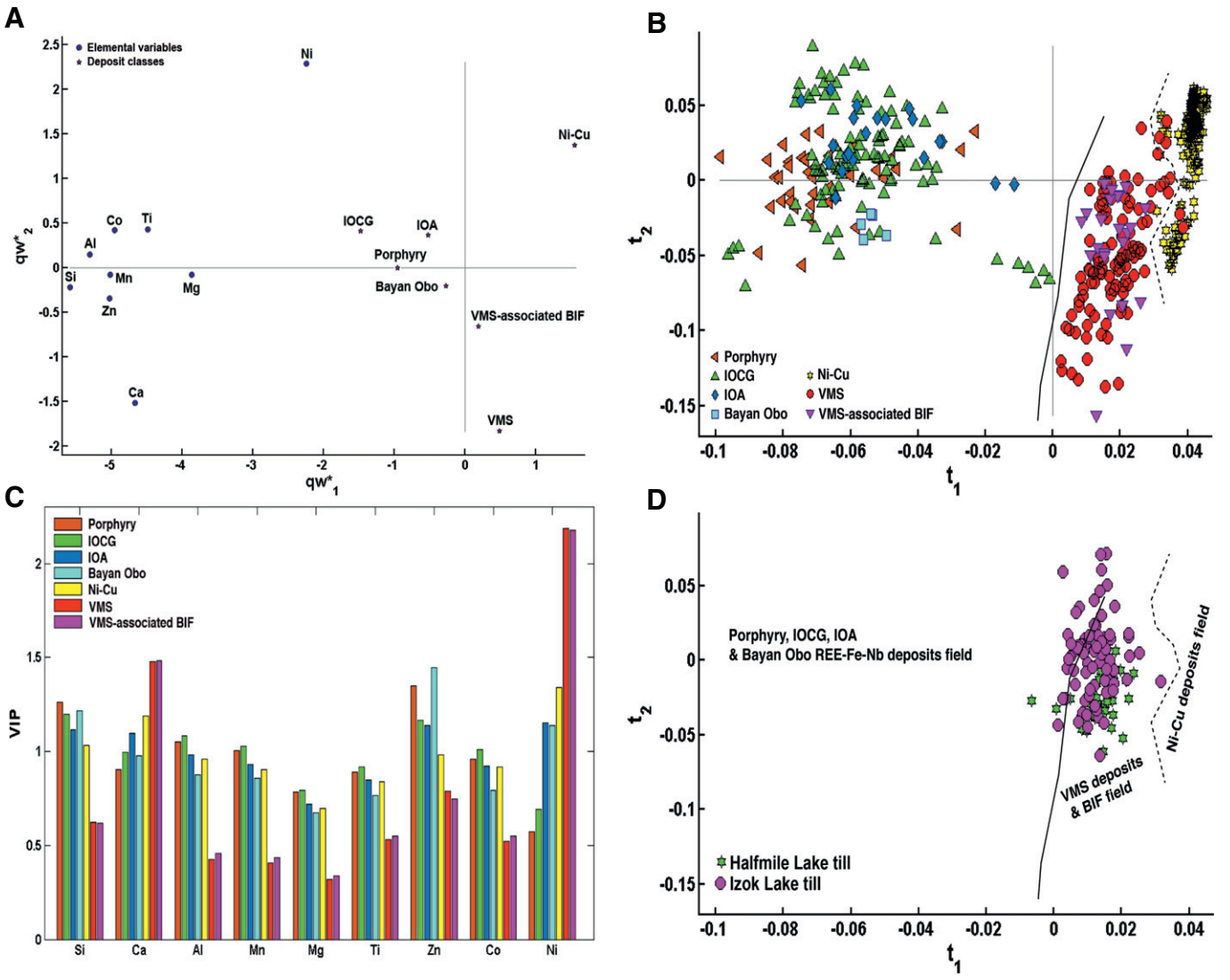

Fig. 7. PLS-DA of LA-ICP-MS data for magnetite from various ore deposit types including VMS, VMS-associated BIF, Ni–Cu, IOCG, IOA, porphyry and the Bayan Obo REE-Fe-Nb deposit. **A)** $\mathbf{qw^*_1}$-$\mathbf{qw^*_2}$ (first and second loadings) shows correlations among elemental variables and deposit classes. **B)** The $\mathbf{t_1}$-$\mathbf{t_2}$ (first and second scores) plot shows the distribution of magnetite analyses from different VMS deposits in the latent variable space defined by $\mathbf{qw^*_1}$-$\mathbf{qw^*_2}$. The solid line in **B** limits the field for VMS and VMS-associated BIFs, whereas a dashed line limits the field for Ni–Cu deposits. **C)** The VIP showing the importance of compositional variables in classification of samples in **B**. Deposits and bedrock lithologies are numbered in **C** to facilitate searching corresponding VIP values. **D)** Projection of the compositional data of detrital magnetite grains from the Haflmile Lake and Izok Lake areas into **B**.

(Fig. 2E), Amulet, Izok Lake (Fig. 2F), and Lasail samples suggest that the iron oxide might form at the expense of massive sulfides and silicates. In deposits other than Izok Lake and Amulet, magnetite is intergrown with the assemblage chlorite ± sericite ± quartz ± calcite ± epidote (Table 3) that indicates that the iron oxide, at least in part, grew during greenschist facies metamorphism. The metamorphic magnetite from these VMS deposits is commonly depleted in Si, Ca, Al, Mg, Ti and Ni, but rich in Mn (Table 2). Manganese might be incorporated into magnetite during diffusion and redistribution of elements between coexisting oxides and mafic silicates during metamorphism (Cassidy et al., 1988; Zaccarini et al., 2004).

In comparison with hydrothermal magnetite from the Horne, Normetal, Turgeon and Little Bay deposits, the majority of metamorphic magnetite is enriched in Zn and/or Co (Table 2). Nadoll et al. (2012) studied various types of magnetite from hydrothermal deposits and host rocks of the Mesoproterozoic Belt Supergroup (United States), and showed that magnetite from the burial metamorphic host rocks as well as the sediment-hosted Cu–Ag deposits is rich in Zn, whereas magmatic magnetite from the Coeur d'Alene host rocks are rich in Co. Thus, the Zn or Co enrichments as well as chalcopyrite and/or sphalerite inclusions in metamorphic magnetite from the VMS deposits such as Lac Dufault (Fig. 2C; Table 3) suggest that the composition of magnetite might be controlled by the composition of precursor Zn- or Co-bearing sulfides, or magma-derived hydrothermal fluids. In the Brunswick #6 (Fig. 2E) and Brunswick #12 deposits, the euhedral form of magnetite aggregates and equilibrium boundaries between magnetite and the associated, metamorphic assemblage chlorite-quartz suggest that magnetite recrystallized during metamorphism. Galena inclusions also indicate that magnetite formed by replacing *pre*-existing sulfides. Similar petrographic and chemical characteristics of magnetite from the Brunswick #6 and Brunswick #12 deposits (Table 3; Figs. 4A-C and 5A-C) demonstrate that in these deposits magnetite was crystallized from the same hydrothermal fluid sources and/or under the same physicochemical conditions.

In the Izok Lake deposit, intergrowths of magnetite and actinolite reveal that the iron oxide formed during the amphibolite facies metamorphism (Fig. 2F). Magnesioferrite exsolution characterizing Izok Lake magnetite (Fig. 2F) also indicates formation of the precursor spinel at high temperatures, consistent with the amphibolite facies metamorphism and subsequent slow cooling (Makvandi et al., 2016). On the basis of grain

morphology, surface textures, and the composition of mineral associations, Makvandi et al. (2015) suggested a metamorphic origin for magnetite in the Izok Lake deposit. In the Amulet deposit, intergrowths of magnetite and anthophyllite also suggest a metamorphic origin for magnetite. Anthophyllite is a magnesium-iron orthoamphibole, favored in low-pressure and high-temperature conditions. At Amulet, anthophyllite and cordierite partly replaced chlorite and quartz during contact metamorphism to the amphibolite facies caused by the intrusion of the nearby Lac Dufault granodiorite (Hall, 1982; Beaty and Taylor, 1982). High Zn, and low Al and Ti are the main contributors plotting Izok Lake and Amulet magnetite in the vicinity of each other in Fig. 4A. This similar chemistry can be explained by similar physicochemical conditions under which magnetite from these deposits grew. At Izok Lake and Amulet, both VMS deposits are hosted by andesite-dacite Archean volcanic rocks that were affected by metamorphism to the amphibolite facies (Morrison, 2004; Gibson et al., 1983). Both VMS deposits are also enclosed by Mg-rich and Na-depleted alteration zones (Morrison, 2004; Gibson et al., 1983). In addition, metamorphic magnetite from the Izok Lake and Amulet deposits formed by replacing sulfides, mostly chalcopyrite and sphalerite (Fig. 2F).

Boutroy et al. (in press) identified veins of magnetite that crosscut and partly replaced pyrrhotite or chalcopyrite in semi-massive and disseminated sulfide bodies associated with Ni–Cu deposits. Their results showed that sulfides replaced by magnetite is relatively depleted in Al, Mn, Ti, V and Cr, and enriched in Si, Ca and Mg. Unlike Ni–Cu deposits, in VMS deposits, both types of magnetite that either replaced or is intergrown with sulfides are mostly depleted in Si, Ca, Zr, Al and Mg, but enriched in Mn (Table 2). Differences in chemistry of magnetite from VMS deposits and that from Ni–Cu deposits can be explained by 1) different compositions of parental hydrothermal fluids, host bedrocks, and co-forming minerals controlling the availability of trace elements as well as their partitioning behavior in magnetite, and 2) different physicochemical conditions (e.g., redox, temperature, pressure, pH) at the time of magnetite formation (Boutroy et al., in press; Dare et al., 2014; Nadoll et al., 2014).

5.1.2. Zoned magnetite at west Ansil

In the West Ansil deposit, massive magnetite widely occurs in the massive sulfide lenses, and replaced pyrrhotite and chalcopyrite (Westendrop et al., 1991; Galley et al., 2000; Boucher, 2011). Boucher (2011) recognized two stages of mineralization at West Ansil, such that, in the first stage, sphalerite, pyrrhotite, and subordinate pyrite were mineralized during the chlorite-quartz alteration, whereas in the latter stage, pyrrhotite and chalcopyrite were mineralized, and later replaced by magnetite. At West Ansil, a decrease in the temperature from 400 to 200 °C, as well as an increase in oxygen fugacity of high-temperature hydrothermal fluids, might result in destruction of chalcopyrite and pyrrhotite, and their replacement by magnetite (Riverin et al., 1990; Barrett et al., 1991). Boucher (2011) suggested that quartz-magnetite veins characterizing the hanging wall of the West Ansil Upper lens precipitated from hydrothermal fluids after burial of the deposit. Galley et al. (2000) proposed that the chalcopyrite replacement by magnetite at West Ansil has resulted in remobilization of Cu, and consequent deposition of prograde sulfide ores. The replacement of pyrrhotite and chalcopyrite by massive magnetite might produce abundant open spaces, as a result of a negative change in molar volume, which were filled by quartz, chlorite and remobilized pyrrhotite and chalcopyrite (Fig. 2G; de Rosen-Spence, 1976; Barrett et al., 1991; Boucher, 2011).

In the West Ansil deposit, magnetite is characterized by growth zoning (Fig. 3A-C). Blenkinsop (2000) demonstrated that growth zoning might occur at constant temperature and pressure because of preferential partitioning of an element into a mineral during its growth. However, growth zoning is commonly cited as the result of changes in fluid compositions and/or physicochemical parameters (such as temperature and oxygen fugacity) during crystal growth, which periodically affect the partitioning behavior of trace elements into magnetite and co-forming minerals (Shimazaki, 1998; Blenkinsop, 2000; Dare et al., 2014). As shown in Fig. 3A and B, West Ansil zoned magnetite consists of a core of inclusion-free magnetite rimmed by silica-rich magnetite. Remobilization of trace elements during the replacement of massive sulfides by magnetite might form the cores free of trace elements (e.g., Boucher, 2011), whereas, the Si enrichment in magnetite rims could be either the consequence of the replacement of pre-existing quartz gangue in the massive pyrrhotite ore (Boucher, 2011), or the signature of reaction with Si-rich fluids (Westendrop et al., 1991). Magnetite crystallized from low temperature hydrothermal fluids is most likely depleted in trace elements because of their low solubility in fluids at lower temperatures (e.g., Dare et al., 2014). Dare et al. (2015) showed that oscillatory zoning in magnetite from the El Laco IOA deposit could have resulted from episodic dissolution and re-precipitation of magnetite from high temperature hydrothermal fluids, and incorporation of some elements such as Si, Ca and REEs, released from dissolution of silicates, into magnetite during its precipitation. Reich et al. (2014) showed Ti, V, Al, and Mn zoning in magnetite from the Los Colorados iron oxide-apatite deposit (Chile) such that the concentration of these elements decreases significantly from core to rim. They suggested that the core magnetite was magmatic in origin, whereas the rim magnetite formed as a result of hydrothermal alteration of magmatic magnetite and consequent remobilization of trace elements.

5.1.3. Metamorphic magnetite in VMS-associated BIFs

Magnetite is a major constituent of iron formations, and may form by recrystallization of precursor magnetite, hematite and/or silicates (Klein, 2005). In the Izok Lake silicate facies BIF, anhedral, fine-grained magnetite is commonly intergrown with biotite and hornblende (Fig. 2H), and to a less extent with almandine (Table 3; Makvandi et al., 2016). Fyfe and Turner (1966) showed that hornblende, biotite, and subordinate magnetite are common in an amphibolite facies mineral assemblage after basic volcanic rocks. Magnetite may form by decomposition of Fe-bearing silicates during metamorphism (Nesbitt, 1986; Bekker et al., 2010). The magnetite-almandine intergrowth can be indicative of destabilization of a high temperature precursor during metamorphism resulting in exsolution of magnetite from almandine (Brearely and Champness, 1986). Izok-silicate facies BIF-mag is enriched in Ti, Al, and Ni (Table 3). This chemistry can be inherited from replaced minerals or high temperature precursors (e.g., Nielsen et al., 1994; Toplis and Carroll, 1995; Nadoll et al., 2014). Although elements such as Ti and Al that are commonly immobile in most altered and metamorphosed rocks, they have migrated locally and redistributed between coexisting minerals during chlorite alteration (Campbell et al., 1984; Whitford et al., 1988; Bau, 1991; Valsami and Cann, 1992), and/or at low grade metamorphism (Evans and Frost, 1975; van Baalen, 1993). Chung et al. (2015) also showed enrichment in Ti and Al characterizing hydrothermal magnetite from the late Paleoproterozoic Sokoman iron formation (Labrador, Canada). They suggested that Sokoman magnetite formed by recrystallization of sedimentary precursor magnetite during interaction with hydrothermal fluids during low-grade metamorphism. Chung et al. (2015) indicated that in comparison with other types of magnetite characterizing the Sokoman iron formation (such as primary and volcanic breccia associated magnetite), the hydrothermal variety has wider range of Ti, Al, Mg, Mn, V, Cr, Co and Zn compositions. They concluded that variable contribution of the host mafic-ultramafic intrusions and different hydrothermal fluids were responsible for formation of each type of magnetite and their highly variable trace elemental contents in the Sokoman iron formation.

In the Austin Brook oxide- and sulfide-facies BIFs, cubic, fine- to medium-grained magnetite is associated with the low-grade metamorphic assemblage chlorite ± siderite ± sericite (Fig. 2I and J; Table 3). Inclusions of these minerals in magnetite and the replacement of magnetite edges by these minerals (Fig. 2I and J) suggest that BIF-mag

formed during metamorphism, however, changes to physicochemical parameters (e.g., temperature, pH, oxygen fugacity) most probably formed metamorphic minerals that replaced magnetite. In the Austin Brook oxide-facies BIF, the abundance of fine-grained hematite associated with magnetite association (Fig. 2I) is further evidence for variable physicochemical conditions affecting the host bedrocks. Lentz and McCutcheon (2006) suggested that, at Austin Brook, hematite formed by replacing magnetite. In the majority of metamorphosed BIFs, magnetite and hematite commonly occur together, though magnetite is mostly present in deeper zones to prevent replacement by pervasive oxidation (Taylor et al., 2001; Mukhopadhyay et al., 2008; Duuring and Hagemann, 2012; Nadoll et al., 2014). Hematite pseudomorphs are common supergene alteration products after magnetite in iron deposits as reported for sub-Phanerozoic BIFs such as Kelsey Lake, Irex-Choiceland and Ipsco in the Choiceland area (e.g., Cheesman, 1964; Thurston and Rogers, 1995). Magnetite and hematite commonly form in the early stages of diagenesis of an iron formation (Klein, 2005). Morris (1980) showed that the Brockman iron formation (Hamersley Province, Western Australia) is characterized by different stages of magnetite and hematite crystallization, as fine-grained hematite is overgrown by diagenetic magnetite, which in turn, is overprinted by crystallization of postmetamorphic hematite. Table 2 shows that Austin-oxide facies BIF-mag contains higher amounts of Mn (0.2 wt.%) than magnetite from the other deposits suggesting that magnetite fingerprints strong Mn enrichment in the exhalite horizon comprising the Brunswick massive sulfide deposits and associated iron formations (Lentz and McCutcheon, 2006). In contrast, Austin-sulfide facies BIF-mag contains higher amounts of Ca (0.8 wt.%) compared to magnetite from the other deposits. The Ca enrichment might be explained by the chemistry of Ca-bearing silicates/carbonates replaced by magnetite either during diagenesis or metamorphism (Lentz and McCutcheon, 2006), or it has a hydrothermal origin (Nadoll et al., 2014; Dare et al., 2014).

5.1.4. Magmatic magnetite in VMS deposits host rocks

Petrography reveals that the Halfmile Lake gossans (Makvandi et al., 2016), Amulet dalmatianite (Fig. 2K), as well as the Quemont (Fig. 2L) and Poirier diabasic host bedrocks contain magmatic magnetite (Table 3). Intergrowths of magnetite and ilmenite lamellae are common characteristics of magnetite formed in magmatic systems, as ilmenite exsolves from magnetite during slow cooling of a higher temperature spinel (Kolker, 1982; von Gruenewaldt et al., 1985; Pang et al., 2008; Liu et al., 2015). Enrichment of Ti, and Zn or Ni in the magmatic magnetite from the studied VMS settings (Fig. 4A; Table 3) is consistent with their crystallization from high-temperature magmas (Dare et al., 2014; Nadoll et al., 2014). The presence of chlorite, sericite, anthophyllite, and biotite, the major constituents of the Amulet dalmatianite (Fig. 2K; Gibson et al., 1983), in association with magmatic magnetite suggests that primary mineral associations of magnetite were obliterated during the amphibolite facies contact metamorphism and hydrothermal alteration. In contrast to Amulet dalmatianite magnetite, magmatic magnetite from the Halfmile Lake gossans, and the Quemont (Fig. 2L) and Poirier diabasic host bedrocks was partly replaced by the assemblage chlorite + calcite + sericite ± quartz (Table 3) that suggests the host bedrocks were subjected to the greenschist facies metamorphism.

5.2. Discriminating different VMS settings by PLS-DA of magnetite composition

Conventional statistical methods such as binary diagrams are appropriate for small datasets where limited number of variables can be selected to show covariation of data (Nguyen and Rocke, 2002). In contrast, PLS-DA is a multivariate statistical method adapted for high dimensional sample classification (Wold, 1966; Barker and Rayens, 2003). PLS-DA identifies Si, Ca, Zr, Al, Mg, Ti, Zn, Co and Ni as discriminator elements for magmatic magnetite associated with VMS deposits (Figs. 4C and 5C). It also detects useful elements for sample classification regardless of their concentration values in magnetite. For instance, magnetite from all VMS deposits (except for Normetal) and BIFs are enriched in variable contents of Mn (Table 2), however, Figs. 4C and 5C reveal that this element dose not contribute to discriminate different compositions of magnetite.

Fig. 4A also shows positive correlation between Si, Ca and Mg in the composition of magnetite from the studied VMS settings. Nadoll et al. (2012) suggested that high Si, Mg, Al, Ca, and/or Mn values and positive correlation among them indicate contamination of magnetite analyses from micro-inclusions. However, Hu et al. (2014) showed that Si^{4+} and Al^{3+} could be incorporated into the intracrystalline sites of magnetite and substitute Fe^{3+}. Divalent elements such as Mg, Mn and Ca are consequently added to the composition of Si-rich magnetite as a valence state balance related to the substitution of Si^{4+} for Fe^{3+}. Hu et al. (2014) indicated that divalent elements such as Mg^{2+} can directly substitute Fe^{2+} in Si-poor magnetite.

PLS-DA of magnetite compositions from various VMS deposits, host bedrocks, and VMS-associated BIFs (Fig. 4A-C) indicates that magnetite of the same type (e.g., magmatic), but from different deposits show similar chemistry clustering them in the vicinity of each other in $\mathbf{t_1}$-$\mathbf{t_2}$ space. For instance, magmatic magnetite from the Halfmile Lake gossans, and the Amulet dalmatianite, Quemont and Poirier diabasic host bedrocks plot in the high $\mathbf{t_1}$ region in Fig. 4B mainly because of higher Ti and Ni, and lower Si, Ca and Mg. An inverse chemical covariation isolates the zoned magnetite from the West Ansil deposit in opposite side of PLS-DA score plot (Fig. 4B). Hydrothermal magnetite from different VMS deposits and BIFs overlap in $\mathbf{t_1}$-$\mathbf{t_2}$ space and are scattered in the space between magmatic and zoned magnetite (Fig. 4B). However, similar chemistry clusters hydrothermal magnetite from the Izok-silicate facies and Austin-sulfide facies BIFs, that of the Turgeon and Little Bay mafic VMS deposits as well as magnetite from the Brunswick #6 and Brunswick #12 felsic-siliciclastic VMS deposits in close proximity to each other (Fig. 4B). Unlike Izok-silicate facies and Austin-sulfide facies BIF-mag, which are rich in Al and Ti, magnetite from the Austin-oxide facies is discriminated in the $\mathbf{t_1}$-$\mathbf{t_2}$ space because of its high Zn and low Al and Ti (Fig. 4A and B). The PLS-DA suggests that Al, Ti and Zn are the most important variables in classification of BIF-mag (Fig. 4C; Table 3).

Fig. 5A-C display the ability of PLS-DA to discriminate between different types of magnetite and/or deposits in a geologic setting such as the Bathurst mining camp. Magmatic magnetite from the Halfmile Lake gossans is separated from hydrothermal samples in the $\mathbf{t_1}$-$\mathbf{t_2}$ plot (Fig. 5B) due to its higher Al, Ti, Co and Ni, and lower Si, Ca, Zr and Mg contents (Fig. 5A), whereas hydrothermal magnetite from the Turgeon deposit is discriminated by high Mg and Ca values, which fingerprint the host mafic volcanic rocks. Among different samples from the BMC, magnetite from the Brunswick #6 and Brunswick #12 felsic-siliciclastic VMS deposits show similar chemistry resulting in overlapping clusters in Fig. 5B. Higher Si, Zr and Zn, and lower Al and Ti (Fig. 5A and C) relative to the average of the BMC deposits magnetite dataset separate magnetite from the felsic-siliciclastic VMS deposits. In contrast to magnetite from the Brunswick deposits, separation of Austin-oxide facies and Austin-sulfide facies BIF-mag in PLS-DA scores plot (Fig. 5B) indicates that they might be the product of different hydrothermal fluids (Bhattacharya et al., 2007; Chung et al., 2015), or due to changing water depth and/or redox conditions, which is responsible for lateral zoning in some Archaean or Algoma type BIFs and consequent deposition of oxide-, carbonate- and sulfide-bearing sediments (Goodwin, 1973; James, 1983).

Comparing PLS-DA results of LA-ICP-MS data (Figs. 4A-C and 5A-C) with that of EPMA (Fig. 6A-C) demonstrates that a more sophisticated sample classification of a highly correlated dataset requires analyzing more chemical elements. The scattering of different samples in PLS-DA of EPMA data (Fig. 6B) indicates that different VMS subtypes cannot be well classified based on Si, Al, Mn and Mg contents of magnetite. However, Fig. 6A suggests that magnetite from the bimodal-felsic VMS

deposits can be discriminated from that of the other subtypes mainly because of its lower Si content. The VIP plot (Fig. 6C) also confirms that Si is not discriminant for magnetite from bimodal-felsic deposits. In Fig. 6B, magnetite from the GP4F deposit is well classified from that of the other deposits because of its higher Mn and Al and lower Mg and Si values. Magnetite from the GP4F and Kudz Ze Kayah bimodal-felsic deposits, both hosted by the Finlayson Lake district of the Yukon-Tanana terrane (central Yukon Territory; Piercey et al., 2001) plot in the vicinity of each other in $\mathbf{t_1}$-$\mathbf{t_2}$ space (Fig. 6B). Magnetite from the Izok Lake deposit shows wider range of Si, Al, Mn and Mg contents (Fig. 6B) relative to that of the other VMS deposits. However, the mean composition of the Izok Lake cluster is isolated from that of the other deposits by high Mn and Mg, and low Si and Al values (Fig. 6A). Plotting magnetite from the Amulet bimodal-mafic deposit in the field for Izok Lake magnetite (Fig. 6B) emphasizes that the temperature is an important factor controlling the trace element contents of metamorphosed hydrothermal magnetite.

5.3. Discriminating different mineral deposit types based on magnetite composition

The PLS-DA results display that in addition to distinguishing compositions of magnetite from different VMS settings, the chemistry of magnetite is useful to discriminate between VMS deposits and other ore deposit types (Fig. 7A-C). As a result, Ni and Ca contribute greatly to separate VMS and BIF magnetite from that of the other mineral deposit types (Fig. 7C). PLS-DA shows that although magnetite from the VMS deposits and VMS-associated BIFs are characterized by lower values of all elemental variables relative to that of the Ni–Cu, porphyry, IOCG, IOA and Bayan Obo groups (Fig. 7A), they are well classified in $\mathbf{t_1}$-$\mathbf{t_2}$ subspace (Fig. 7B). PLS-DA classified magnetite from Ni–Cu deposits based on their Ni content (Fig. 7A and C). Dare et al. (2012, 2014) and Boutroy et al. (in press) showed that Ni and Cr are compatible into magnetite at different stages of the crystallization of a sulfide melt such that the Ni + Cr content of magnetite is always high in Ni–Cu deposits. The Ni + Cr vs. Si + Mg diagram established by Dupuis and Beaudoin (2011) also separates magnetite from Ni–Cu deposits from that of the other deposit types based on its enrichment in Ni and Cr, and depletion in Si and Mg.

Despite the overlap in clusters of compositions of magnetite in Fig. 7B, the cluster of data for IOCG deposits is separated from those of the other deposit types because of higher Si values (Fig. 7A; Appendix-VI B). Dare et al. (2015) showed that magnetite from the El Laco IOA deposit is enriched in Si, Ca, Na, P and REEs, but depleted in Ti, Al, Cr, Zr, Hf and Sc suggesting its crystallization from high temperature (> 500 °C) hydrothermal fluids. Hitzman et al. (1992) also found out that magnetite from IOCG deposits is commonly depleted in Ti. Boutroy et al. (2012b) compared the compositions of magnetite from Ni-Cu-PGE and IOCG deposits and pointed out that primary magnetite from Ni-Cu-PGE deposits contains higher amounts of Ni, Cu and Cr, and lower concentrations of Ti, Al and Si relative to ore-stage magnetite from IOCG deposits.

Magnetite from the IOA deposits can be discriminated from that of other deposit types due to their higher Ti and Co values (Fig. 7A and C; Appendix-VI C). The IOA magnetite also contains higher Ni content relative to magnetite from the other deposit types other than Ni–Cu deposits. Boutroy et al. (2012b) showed that magnetite from IOA deposits is rich in Al and Mg or in Ca. Knipping et al. (2015) investigated trace element contents of magnetite from the Cretaceous Kiruna-type Los Colorados IOA deposit (Chile), and showed that the chemistry of Los Colorados magnetite is similar to that from high temperature hydrothermal systems, such as porphyry Cu deposits, in which magnetite contains high concentrations of Al, Ti, V and Ga.

Higher Ca content relative to the other deposit types is the main contributor clustering the Bayan Obo REE-Fe-Nb magnetite in the left side of $\mathbf{t_1}$-$\mathbf{t_2}$ (Fig. 7A and B). Huang et al. (2015), however, did not used the Ca content of magnetite in characterizing different types of magnetite associated with the Bayan Obo deposit. They excluded some elements such as Ca from their analyses because their concentrations were close to or below the detection limit of the LA-ICP-MS they used, or because of considerable variation in their contents. The VIP plot) reveals that Si, Ca, Al, Mn, Zn, Co and Ni are discriminator elements for magnetite from various mineral deposit types, whereas Mg and Ti are not useful (Fig. 7C).

5.4. Application of magnetite composition to provenance studies and mineral exploration

Makvandi et al. (2016) used latent variable spaces defined by PCA of the composition of magnetite from the Izok Lake and Halfmile Lake VMS deposits and their host bedrocks to distinguish the sources of iron oxide in local till. To extend Makvandi et al. (2016) studies, the present study provides new datasets of magnetite trace element compositions from various VMS deposits, host bedrocks and VMS-associated BIFs; and also introduces a sophisticated classification technique, PLS-DA, for the provenance identification of detrital magnetite, and consequently for the exploration of VMS deposits hidden under thick layers of overburden. As shown in Appendix-II, PLS-DA offers better classification of samples (Figs. C and D) in comparison with unsupervised PCA (Figs. A and B). For instance, as shown in Appendix-II, magnetite from the West Ansil deposit that forms a distinct cluster in Figure D (PLS-DA scores plot) overlaps the fields for magnetite from the other deposits in Figure B (PCA scores plot). This is because that PCA projects maximum variation in the predictive matrix ($\mathbf{X}$), whereas PLS-DA projects maximum separation between classes in $\mathbf{X}$ (Antti et al., 2004). The PCA and PLS-DA results could be similar if maximum variation in the data was the main source of samples discrimination. Another advantage of using PLS-DA over PCA is the possibility of summarizing the importance of variables in sample classification in VIP plots.

The present study shows that to identify the origin of detrital magnetite in VMS settings, or detect chemical signatures of VMS deposits in unconsolidated sediments, a database of magnetite compositions from VMS deposits (e.g., including data from this study, Makvandi et al., 2016, and Dupuis and Beaudoin, 2011) must be analyzed by PLS-DA to create discrimination models, and then detrital magnetite data should be projected into the models. For instance, Fig. 5D shows that the projection of till magnetite data from the Halfmile Lake area (Makvandi et al., 2016) into the latent variable spaces defined by PLS-DA of magnetite compositions from different VMS deposits and BIFs in the Bathurst district results in plotting the majority of till grains into the field for magmatic magnetite from the Halfmile Lake gossan or close to the field boundaries. This is consistent with the results of Makvandi et al. (2016) indicating that a high proportion of Halfmile Lake till magnetite grains were derived from local igneous bedrocks. Fig. 7D also shows that the projection of the till data from the Izok Lake and Halfmile Lake VMS areas (Makvandi et al., 2016) into PLS-DA subspace estimated using magnetite data from various mineral deposit types (Fig. 7B), results in clustering of a high proportion of till grains in the same region as for the VMS deposits and VMS-associated BIFs. Plotting a low proportion of till magnetite outside, but very close to the boundaries of the VMS deposits and BIFs field, is also inevitable, because a proportion of till magnetite from both VMS settings were derived from host bedrocks or other unclassified rocks (Makvandi et al., 2016). Overall, the results in Figs. 5D and 7D exemplify the potential of magnetite chemistry in provenance studies and exploration for VMS deposits. More specifically, these results demonstrate the utility of PLS-DA for estimating the nature of the bedrock source for magnetite in unconsolidated sediments for which the bedrock source is unknown. Given that magnetite is usually a significant proportion of the heavy mineral concentrate of a till or stream sediment sample, the methods of this study could be applied to magnetite grains in these sediments to screen for the potential presence of mineral deposits in the area.

6. Conclusions

This study documented geochemical characteristics of magnetite from different VMS deposit subtypes, host bedrocks, and VMS-associated BIFs, and identified three types of magnetite associated with VMS settings: magmatic, hydrothermal, and metamorphic. Petrography reveals that in some VMS deposits such as Horne, Normetal, Turgeon, and Little Bay, magnetite precipitated from hydrothermal fluids along with sulfide mineralization, whereas in some other VMS deposits such as Lac Dufault, Amulet, Bell-Allard, Lasail, Brunswick #12, Brunswick #6 and Izok Lake, magnetite is metamorphic in origin. The metamorphic magnetite formed by replacing sulfides, and is intergrown with the assemblage chlorite ± calcite ± sericite ± quartz ± biotite ± anthophyllite. The composition of hydrothermal and metamorphic magnetite associated with massive sulfides is variable, though both types are enriched in Mn, and mostly depleted in Si, Ca, Zr, Al, Ti, and Ni. Enrichment of some magnetite in Ti, Co and/or Zn suggests their crystallization from high temperature hydrothermal fluids or during high-grade metamorphism. It may also fingerprint the chemistry of sulfides or silicates replaced by magnetite.

The Izok Lake and Austin Brook sulfide- and oxide- facies BIFs contain metamorphic magnetite. BIF-mag may form during metamorphism or early stages of diagenesis by decomposition of Fe-bearing silicates during metamorphism, or exsolution from almandine during slow cooling of a high temperature precursor. PLS-DA identifies Al, Ti and Zn as main contributors in the classification of BIF-mag.

Magmatic magnetite from the Halfmile Lake gossans, Amulet dalmatianite, and the Quemont, Poirier diabasic host bedrocks is characterized by ilmenite exsolution, and contains a higher concentration of Ti relative to the other types of magnetite. Magmatic magnetite is commonly rich in Mn, Zn, Co, and/or Ni.

PLS-DA classifies different types of VMS deposits and VMS-associated BIFs using Si, Ca, Zr, Al, Mg, Ti, Zn, Co and Ni contents of magnetite. PLS-DA also distinguished VMS deposits and VMS-associated BIFs from Ni–Cu, IOCG, IOA, and porphyry deposits based on the distribution of Si, Ca, Al, Mn, Mg, Ti, Zn, Co and Ni in magnetite. PLS-DA also yields discrimination models to identify the sources of detrital magnetite in unconsolidated sediments.

Supplementary data to this article can be found online at http://dx.doi.org/10.1016/j.oregeorev.2016.04.014.

Acknowledgements

This research was funded by the joint grant # CRDPJ 392812 a partnership between the Geological Survey of Canada under its Geomapping for Energy and Minerals 1 (GEM 1) Program (2008–2013), Natural Science and Engineering Research Council (NSERC) of Canada, and industrial partners Overburden Drilling Management Limited, MMG Limited, Teck Resources Limited, and AREVA Resources Canada. We would like to thank all who collaborated on this project: M. Choquette (Laval), S.A.S. Dare (uOttawa), M. Javidani (Laval), D. Savard (UQAC), and S. Mehdi (UQAC). Paul Spry (Iowa State University) and an anonymous reviewer are thanked for their insightful reviews of this manuscript.

References

Adair, R.N., 1992. Stratigraphy, structure, and geochemistry of the Halfmile Lake massive-sulfide deposit, New Brunswick. Explor. Min. Geol. 1, 151–166.

Agranier, A., Lee, C.-T.A., Li, X.A., Leeman, W.P., 2007. Fluid mobile element budgets in serpentinized oceanic lithospheric mantle: insights from B, As, Li, Pb, PGEs, and Os isotopes in the Feather River ophiolite, California. Chem. Geol. 245, 230–241. http://dx.doi.org/10.1016/j.chemgeo.2007.08.008.

Aitchison, J., 1986. The Statistical Analysis of Compositional Data. Monographs on Statistics and Applied ProbabilityChapman and Hall Ltd. (Reprinted 2003 with additional material by The Blackburn Press), London (UK) (416 pp.).

Alabaster, T., Pearce, J.A., 1985. The interrelationship between magmatic and ore-forming hydrothermal processes in the Oman ophiolite. Econ. Geol. 80, 1–16.

Antti, H., Ebbels, T.M.D., Keun, H.C., Bollard, M.E., Beckonert, O., Lindon, J.C., Nicholson, J.K., Holmes, H., 2004. Statistical experimental design and partial least squares regression analysis of biofluid metabonomic NMR and clinical chemistry data for screening of adverse drug effects. Chemom. Intell. Lab. Syst. 73 (1), 139–149.

Bacon-Shone, J., 2011. A short history of compositional data analysis. In: Pawlowsky-Glahn, Buccianti (Ed.), Compositional Data Analysis: Theory and Applications. Wiley & Sons, New York (7-11, 378 pp.).

Barker, M., Rayens, W., 2003. Partial least squares for discrimination. J. Chemom. 17 (3), 166–173.

Barrett, T.J., MacLean, W.H., Cattalani, S., 1991. Massive sulfide deposits of the Noranda area Quebec. III. The Ansil mine. Can. J. Earth Sci. 28, 1699–1730.

Bau, M., 1991. Rare-earth element mobility during hydrothermal and metamorphic fluid-rock interaction and the significance of the oxidation state of europium. Chem. Geol. 93, 219–230.

Beaty, D.W., Taylor, H.P., 1982. Some petrologic and oxygen isotopic relationships in the Amulet Mine, Noranda, Quebec, and their bearing on the origin of Archean massive sulfide deposits. Econ. Geol. 77 (1), 95–108.

Beaudoin, G., Dupuis, C., 2009. Iron-oxide trace element fingerprinting of mineral deposit types. In: Mumin, H., Corriveau, L. (Eds.), Exploring for Iron Oxide Copper-Gold Deposits: Canada and Global Analogues, Short Course, Geological Association of Canada Annual Meeting, Québec City, pp. 107–121.

Bekker, A., Slack, J.F., Planavsky, N., Krapez, B., Hofmann, A., Konhauser, K.O., Rouxel, O.J., 2010. Iron Formation: The Sedimentary Product of a Complex Interplay Among Mantle, Tectonic, Oceanic, and Biospheric Processes.

Berzina, A., 2012. Platinum- group element geochemistry of magnetite from porphyry-Cu-Mo deposits and their host rocks (Siberia, Russia). Acta Geol. Sin. 86, 106–117.

Bhattacharya, H.N., Chakrabortym, I., Ghosh, K.K., 2007. Geochemistry of some banded iron-formations of the Archean Supracrustals, Jharkhand-Orissa region, India. J. Earth Syst. Sci. 116, 245–259.

Bleeker, W., Hall, B., 2007. The slave craton: geological and metallogenic evolution. Mineral deposits of Canada: a synthesis of major deposit-types, district metallogeny, the evolution of geological provinces, and exploration methods. In: Goodfellow, W.D. (Ed.)Geological Association of Canada, Mineral Deposits Division, Special Publication Vol. 5, pp. 849–879.

Bleeker, W., Ketchum, J.W.F., Davis, W.J., 1999. The central slave basement complex, part II: age and tectonic significance of highstrain zones along the basement-cover contact. Can. J. Earth Sci. 36, 1111–1130.

Blenkinsop, T.G., 2000. Deformation Microstructures and Mechanisms in Minerals and Rocks. Springer, Netherlands http://dx.doi.org/10.1007/0-306-47543-X (150 pp.).

Boucher, S.M., 2011. Ore petrology and alteration of the West Ansil volcanic-hosted massive sulphide deposit of the Noranda Mining Camp, Rouyn-Noranda, Québec (Master of science Thesis) Department of Earth Sciences, University of Ottawa, Canada (193 pp.).

Boutroy, 2013. Magnetite from Porphyry Deposits. NSERC-AEM Chair Mineral Exploration Workshop. Université Laval, Quebec, Canada.

Boutroy, E., Dare, S.A.S., Beaudoin, G., Barnes, S.J., 2012a. Minor and trace element composition of magnetite from Ni-Cu deposits worldwide and its application to mineral exploration. GAC-MAC 2012, St- John's, NL, Canada.

Boutroy, E., Beaudoin, G., Barnes, S.J., Corriveau, L., 2012b. Minor and Trace Element Composition of Iron Oxides from IOCG Deposits Worldwide and its Application to Mineral Exploration. Goldschmidt Conference 2012, Montreal, Canada.

Boutroy, E., Dare, S.A.S., Beaudoin, G., Barnes, S.J., Lightfoot, P.C., 2014. Minor and trace element composition of magnetite from Ni-Cu-PGE deposits worldwide and its application to mineral exploration. J. Geochem. Explor. 145, 64–81.

Bowles, J.F.W., Howie, R.A., Vaughan, D.J., Zussman, J., 2011. Rock-forming Minerals-Non-silicates: oxides, hydroxides and sulphides. second ed. Geological Society, London.

Boyle, D.R., 2003. Preglacial weathering of massive sulphide deposits in the Bathurst Mining Camp: economic geology, geochemistry, and exploration applications. In: Goodfellow, W.D., McCutcheon, S.R., Peter, J.M. (Eds.), Massive Sulphide Deposits of the Bathurst Mining Camp, New Brunswick, and Northern Maine. Society of Economic Geologists, Monograph Vol. 11, pp. 689–721.

Brearely, A.J., Champness, P.E., 1986. Magnetite exsolution in almandine garnet. Mineral. Mag. 50, 621–633.

Budulan, G., McClenaghan, M.B., Parkhill, M.A., Layton-Matthews, D., Pyne, M., 2013. Till geochemical signatures of the Halfmile Lake Zn-Pb-Cu volcanogenic massive sulphide deposit, Bathurst Mining Camp, New Brunswick. Geological Survey of Canada Open File 7174 (122 pages).

Budulan, G., McClenaghan, M.B., Layton-Matthews, D., Crabtree, D., Pyne, M., McClenaghan, S., 2015. Indicator mineral signatures of the Halfmile Lake Zn-Pb-Cu volcanogenic massive sulphide deposit, Bathurst Mining Camp, New Brunswick: Part 1- bedrock data. Geological Survey of Canada Open File 7644 (75 pp.).

Campbell, I.H., Lesher, C.M., Coad, P., Franklin, J.M., Gorton, M.P., Thurston, P.C., 1984. Rare-earth element mobility in alteration pipes below massive Cu-Zn sulfide deposits. Chem. Geol. 45, 181–202.

Cassidy, K.F., Groves, D.I., Binns, R.A., 1988. Manganoan ilmenite formed during regional metamorphism of Archean mafic and ultramafic rocks from Western Australia. Can. Mineral. 26, 999–1012.

Cheesman, R.L., 1964. The geology of the Choiceland iron deposit, Saskatchewan. Can. Inst. Min. Metall. Bull. 57, 715–718.

Chen, W.T., Zhou, M.-F., Gao, J.-F., Hu, R., 2015. Geochemistry of magnetite from Fe-Cu deposits in the Kangdian metallogenic province, SW China. Mineral. Deposita http://dx.doi.org/10.1007/s00126-014-0575-7.

Chong, I.G., Jun, C.H., 2005. Performance of some variable selection methods when multicollinearity is present. Chemom. Intell. Lab. Syst. 78, 103–112.

Chung, D., Zhou, M.F., Gao, J.-F., Chen, W.T., 2015. In-situ LA-ICP-MS trace elemental analyses of magnetite: the late Palaeoproterozoic Sokoman iron formation in the Labrador trough, Canada. Ore Geol. Rev. 65, 917–928.
Daigneault, R., Mueller, W.U., Chown, E.H., 2004. Abitibi greenstone belt plate tectonics: the diachronous history of arc development, accretion and collision. In: Eriksson, P.G., Altermann, W., Nelson, D.R., Mueller, W.U., Catuneau, O., Strand, K. (Eds.), Developments in Precambrian Geology/Tempos of Events in Precambrian Time. Elsevier, Amsterdam, pp. 88–103.
Dare, S.A.S., Barnes, S.J., Beaudoin, G., 2012. Geochim. Cosmochim. Acta 88, 27–50.
Dare, S.A.S., Barnes, S.J., Beaudoin, G., Meric, J., Boutroy, E., Potvin-Doucet, C., 2014. Trace elements in magnetite as petrogenetic indicators. Mineral. Deposita 1–12.
Dare, S.A.S., Barnes, S.J., Beaudoin, G., 2015. Did the massive magnetite "lava flows" of El Laco (Chile) form by magmatic or hydrothermal processes? New constraints from magnetite composition by LA-ICP-MS. Miner. Deposita 50 (5), 607–617.
Deer, W.A., Howie, R.A., Zussman, J., 1992. An introduction to the rock-forming minerals. In: Harlow, England (Ed.) Longman Scientific & Technical, p. 695.
de Iorio, M., Ebbels, T.M.D., Stephens, D.A., 2008. Statistical Techniques in Metabolic Profiling. Handbook of Statistical Genetics, third ed., pp. 347–373 http://dx.doi.org/10.1002/9780470061619.ch11.
de Rosen-Spence, A.F., 1976. Stratigraphy, Development and Petrogenesis of the Central Noranda Volcanic Pile, Noranda, Quebec (Ph.D. thesis) University of Toronto, Toronto, Ontario, Canada (166 pp.).
Dimroth, E., Imreh, L., Goulet, N., Rocheleau, M., 1983. Evolution of the south-central segment of the Archean Abitibi Belt, Quebec. Part III: plutonic and metamorphic evolution and geotectonic model. Can. J. Earth Sci. 20, 1374–1388.
Dupuis, C., Beaudoin, G., 2011. Discriminant diagrams for iron oxide trace element fingerprinting of mineral deposit types. Mineral. Deposita 46, 319–335.
Duuring, P., Hagemann, S.G., 2012. Leaching of silica bands and concentration of magnetite in Archean BIF by hypogene fluids: Beebyn Fe ore deposit, Yilgarn Craton, Western Australia. Mineral. Deposita 48, 341–370.
Egozcue, J.J., Pawlowsky-Glahn, V., Mateu-Figueraz, G., Barceló-Vidal, C., 2003. Isometric logratio transformations for compositional data analysis. Math. Geol. 35 (3), 279–300.
Energy, Mines and Resources Canada, 1989. Canadian mineral deposits not being mined in 1989. Mineral Resources Bulletin MR2 223 (400 pp.).
Eriksson, L., Johansson, E., Kettaneh-Wold, N., Wold, S., 2001. Multi- and Megavariate Data Analysis, Principles and Applications. UMETRICS, Umea (425 pp.).
Evans, B.W., Frost, B.R., 1975. Chrome-spinel in progressive metamorphism- a preliminary analysis. Geochim. Cosmochim. Acta 39, 959–972.
Evans D.T.W., Swinden H.S., Kean B.S., Hogan A., 1992. Metallogeny of the vestiges of Iapetus, Island of Newfoundland. Newfoundland Department of Mines and Energy Map 92–19, scale 1:500000.
Filzmoser, P., Hron, K., Reimann, C., 2009. Principal component analysis for compositional data with outliers. Environmetrics 20 (6), 621–632.
Franklin, J.M., Gibson, H.L., Jonasson, I.R., Galley, A.G., 2005. Volcanogenic massive sulfide deposits. Economic Geology 100th Anniversary, pp. 523–560.
Frost, B.R., 1979. Metamorphism of iron-formation; parageneses in the system Fe-Si-C-O-H. Econ. Geol. 74, 775–785.
Fyfe, W.S., Turner, F.J., 1966. Reappraisal of the metamorphic facies concept. Contrib. Mineral. Petrol. 12, 354–364.
Gaboury, D., Pearson, V., 2008. Rhyolite geochemical signatures and association with volcanogenic massive sulfide deposits: examples from the Abitibi Belt, Canada. Econ. Geol. 103 (7), 1531–1562.
Galley, A.G., Jonasson, I.R., Watkinson, D.H., 2000. Magnetite-rich calc-silicate alteration in relation to synvolcanic intrusion at the Ansil volcanogenic massive sulfide deposit, Rouyn-Noranda, Quebec, Canada. Mineral. Deposita 35, 619–637.
Galley, A.G., Hannington, M.D., Jonasson, I.R., 2007. Volcanogenic massive sulfide deposits. Mineral deposits of Canada. In: Goodfellow, W.D. (Ed.), Mineral Deposits of Canada: A Synthesis of Major Deposit-Types, District Metallogeny, the Evolution of Geological Provinces, and Exploration Methods. Geological Association of Canada, Mineral Deposits Division, Special Publication Vol. 5, pp. 141–161.
Geladi, P., Grahn, H., 1996. Multivariate Image Analysis. John Wiley & Sons (330 pp.).
Genna, D., Gaboury, D., Roy, G., 2014. The key tuffite, Matagami Camp, Abitibi Greenstone Belt, Canada: petrogenesis and implications for VMS formation and exploration. Mineral. Deposita 49, 489–512.
Gibson, H.L., Kerr, D.J., 1993. Giant volcanic-associated massive sulphide deposits, with emphasis on Archean examples. Soc. Econ. Geol. Spec. Publ. 2, 319–348.
Gibson, H.L., Watkinson, D.H., 1990. Volcanogenic massive sulphide deposits of the Noranda cauldron and shield volcano, Quebec. Can. Inst. Min. Metall. Spec. 43, 119–132.
Gibson, H.L., Watkinson, D.H., Comba, C.D.A., 1983. Silicification: hydrothermal alteration in an Archean geothermal system within the amulet rhyolite formation, Noranda, Quebec. Econ. Geol. 78, 954–971.
Gilgen, S.A., Diamond, L.W., Mercolli, I., Al-Tobi, K., Maidment, D.W., Close, R., Al-Towaya, A., 2014. Volcanostratigraphic controls on the occurrence of massive sulfide deposits in the Semail Ophiolite, Oman. Econ. Geol. 109, 1585–1610.
Goodfellow, W.D., McCutcheon, S.R., 2003. Geologic and genetic attributes of volcanic sediment-hosted massive sulfide deposits of the Bathurst Mining Camp, northern New Brunswick— a synthesis. Econ. Geol. Monogr. 11, 245–302.
Goodfellow, W.D., McCutcheon, S.R., Peter, J.M., 2003. Massive sulfide deposits of the Bathurst Mining Camp, New Brunswick, and Northern Maine: introduction and summary of findings. Econ. Geol. Monogr. 11, 1–16.
Goodwin, A.M., 1973. Archean iron-formation and tectonic basins of the Canadian shield. Econ. Geol. 68, 915–933.
Grunsky, E.C., 2010. The interpretation of geochemical survey data. Geochem. Explor. Environ. Anal. 10, 27–74.
Grunsky, E.C., Drew, L.J., Woodruff, L.G., Friske, P.W.B., Sutphin, D.M., 2013. Statistical variability of the geochemistry and mineralogy of soils in the maritime provinces of Canada and part of the Northeast United States. Geochem. Explor. Environ. Anal. 13 (4), 249–266.
Hall, B.V., 1982. Geochemistry of the alteration pipe at the Amulet Upper A deposit, Noranda, Quebec. Can. J. Earth Sci. 19, 2060–2084.
Helsel, D.R., 2005. Nondetects and Data Analysis. Wiley, New York (268 pages).
Hitzman, M.W., Oreskes, N., Einaudi, M.T., 1992. Geological characteristics and tectonic setting of Proterozoic iron oxide (Cu-U-Au-REE) deposits. Precambrian Res. 58, 241–287.
Hron, K., Templ, M., Filzmoser, P., 2010. Imputation of missing values for compositional data using classical and robust methods. Computat. Stat. Data Anal. 54 (12), 3095–3107.
Hu, H., Li, J.W., Lentz, D., Ren, Z., Zhao, X.F., Deng, X.D., Hall, D., 2014. Dissolution-reprecipitation process of magnetite from the Chengchao iron deposit: insights into ore genesis and implication for in-situ chemical analysis of magnetite. Ore Geol. Rev. 57, 393–405.
Huang, X., Qi, L., Meng, Y., 2014. The element geochemistry of magnetite from Fe(−Cu) deposits in the Hami Region, Eastern Tianshan Orogenic Belt, NW China. Acta Geol. Sin. 88 (1), 176–195.
Huang, X., Zhou, M.F., Qiu, Y.Y., Qi, L., 2015. In-situ LA-ICP-MS trace elemental analyses of magnetite: the Bayan Obo Fe-REE-Nb deposit, North China. Ore Geol. Rev. 65 (4), 884–899.
Jacob, H.L., Tremblay, A., 2012. Geological description of the Joulet property, Abitibi, Quebec. Consultation Geo-logic, Technical Report NI 43-101 and NI 43-101A (46 pages).
James, H.L., 1983. Distribution of banded iron-formation in space and time. In: Trendall, A.F., Morris, R.C. (Eds.), Iron Formation Facts and Problems. Developments in Precambrian Geology Vol. 6, pp. 471–490.
Jarosewich, E., Nelen, J.A., Norberg, J.A., 1980. Reference samples for electron microprobe analysis. Geostand. Newslett. 4, 43–47.
Kean, B.F., Evans, D.T.W., Jenner, G.A., 1995. Geology and Mineralization of the Lushs Bight Group. Newfoundland and Labrador Department of Natural Resources, Geological Survey, Report 95-02 (204 pages).
Kennedy, L.P., 1985. The geology and geochemistry of the Archean Flavrian pluton, Noranda, Quebec (PhD thesis) University of Western Ontario, London, Ontario (469 pages).
Kettles, K.R., 1987. The Turgeon mafic volcanic associated Fe-Cu-Zn sulphide deposit in the ophiolitic Fournier Group, Northern New Brunswick (M.Sc. thesis) University of New Brunswick, Fredericton (202 pages).
Klein, C., 2005. Some Precambrian banded iron-formations (BIFs) from around the world: their age, geologic setting, mineralogy, metamorphism, geochemistry, and origin. Am. Mineral. 90, 1473–1499.
Knipping, J.L., Bilenker, L.D., Simon, A.C., Reich, M., Barra, F., Deditius, A.P., Heinrich, C.A., Holtz, F., Munizaga, R., 2015. Trace elements in magnetite from massive iron oxide-apatite deposits indicate a combined formation by igneous and magmatic-hydrothermal processes. Geochim. Cosmochim. Acta 171, 15–38.
Kolker, A., 1982. Mineralogy and geochemistry of Fe-Ti oxide and apatite (nelsonite) deposits and evaluation of the liquid immiscibility hypothesis. Econ. Geol. 77, 1146–1158.
Kramer, R., 1998. Chemometric Techniques for Quantitative Analysis. 1 ed. CRC Press (220 pages).
Lalonde, E., Beaudoin, G., 2015. Petrochemistry, hydrothermal alteration, mineralogy, and sulfur isotope geochemistry of the Turgeon Cu-Zn volcanogenic massive sulfide deposit, northern New Brunswick, Canada. Can. J. Earth Sci. 52, 215–234.
Lentz, D., Goodfellow, W.D., 1993. Mineralogy and petrology of the stringer sulphide zone in the Discovery Hole at the Brunswick No. 12 massive sulphide deposit, Bathurst, New Brunswick. Geological Survey of Canada Paper 93-1E, pp. 249–258.
Lentz, D., Goodfellow, W.D., 1996. Intense silicification of footwall sedimentary rocks in the stockwork alteration zone beneath the Brunswick no. 12 massive sulphide deposit, Bathurst, New Brunswick. Can. J. Earth Sci. 33, 284–302.
Lentz, D.R., McCutcheon, S.R., 2006. The Brunswick no. 6 massive sulfide deposit, Bathurst Mining Camp, northern New Brunswick, Canada: a synopsis of the geology and hydrothermal alteration system. Explor. Min. Geol. 15 (3–4), 1–34.
Lindsley, D.H., 1976. The crystal chemistry and structure of oxide minerals as exemplified by the Fe-Ti oxides. In: Rumble III, D. (Ed.), Oxide Minerals. Reviews in Mineralogy: Mineralogical Society of America, pp. L1–L60.
Liu, P.P., Zhou, M.F., Chen, W.T., Gao, J.F., Huang, X.W., 2015. In-situ LA-ICP-MS trace elemental analyses of magnetite: Fe-Ti-(V) oxide-bearing mafic-ultramafic layered intrusions of the Emeishan Large Igneous Province, SW China. Ore Geol. Rev. 65 (4), 853–871.
Loannou, S.E., Spooner, E.T.G., 2007. Fracture analysis of a volcanogenic massive sulfide-related hydrothermal cracking zone, Upper Bell River Complex, Matagami, Quebec: application of permeability tensor theory. Econ. Geol. 102, 667–690.
Longerich, H.P., Jackson, S.E., Günther, D., 1996. Laser ablation-inductively coupled plasma-mass spectrometric transient signal data acquisition and analyte concentration calculation. J. Anal. At. Spectrom. 11, 899–904.
Makvandi, S., Beaudoin, G., McClenaghan, B.M., Layton-Matthews, D., 2015. The surface texture and morphology of magnetite from the Izok Lake volcanogenic massive sulfide deposit and local glacial sediments, Nunavut, Canada: application to mineral exploration. J. Geochem. Explor. 150, 84–103.
Makvandi, S., Ghasemzadeh-Barvarz, M., Beaudoin, G., Grunsky, E.C., McClenaghan, B.M., Duchesne, C., 2016. Principal component analysis of magnetite composition from volcanogenic massive sulfide deposits: case studies from the Izok Lake (Nunavut, Canada) and Halfmile Lake (New Brunswick, Canada) deposits. Ore Geol. Rev. 72, 60–85.
McClenaghan, M.B., Paulen, R.C., Layton-Matthews, D., Hicken, A.K., Averill, S.A., 2015. Glacial dispersal of gahnite from the Izok Lake Zn-Cu-Pb-Ag VMS deposit, Northern Canada. Geochem. Explor. Environ. Anal. http://dx.doi.org/10.1144/geochem2014-317.
McCutcheon, S.R., Walker, J.A., 2001. Volcanogenic massive sulphide deposits of the Bathurst Mining Camp. Geological Association of Canada-Mineralogical Association of

Canada, Joint Annual Meeting, St. John's, Newfoundland, Guidebook for Field Trip B7 (89 pages).
McCutcheon, S.R., Gower, S.J., Lentz, D.R., Langton, J.P., Walker, J.A., Wilson, R.A., Fyffe, L.R., Hamilton, A., Luff, W.M., 1997. Geology and massive sulphides of the Bathurst Camp, New Brunswick. Field Trip B7, Mineralogical Association of Canada Joint Annual Meeting 1997. Canada, Ottawa (91 pages).
McCutcheon, S.R., Walker, J.A., McClenaghan, S.H., 2000. The Geological Setting of Massive Sulphide Deposits in the Bathurst Camp- a Synthesis. New Brunswick Department of Natural Resources and Energy, Minerals and Energy Division, Mineral Resources Report 2001–4, pp. 63–95.
McIntire, W.L., 1963. Trace element partition coefficients— a review of theory and applications to geology. Geochim. Cosmochim. Acta 27, 1209–1264.
Méric, J., 2011. Caractérisation géochimiques des magnétites de la zone critique de l'intrusion magmatique de Sept-Iles (Québec, Canada) et intégration a une base de données utilisant la signature géochimique des oxydes de fer comme outil d'exploration Université duQuébec à Chicoutimi- Université Montpellier Vol. 2 (48 pp.).
Miller, P., Swanson, R., Heckler, C., 1998. Contribution plots: the missing link in multivariate quality control. Appl. Math. Comput. Sci. 8, 775–792.
Ministere des Ressources naturelles du Quebec, 1996 to 2004. Website database, E-sigeom à la carte. http://www.mrn.gouv.qc.ca/english/productsservices/mines.jsp.
Mireku, L.K., Stanley, C.R., 2006. Lithogeochemistry and hydrothermal alteration at the Halfmile Lake south deep zone, a volcanic-hosted massive sulfide deposit, Bathurst Mining Camp, New Brunswick. Explor. Min. Geol. 15 (3–4), 177–199.
Mollo, S., Putirka, K., Iezzi, G., Scarlato, P., 2013. The control of cooling rate on titanomagnetite composition: implications for a geospeedometry model applicable to alkaline rocks from Mt. Etna volcano. Contrib. Mineral. Petrol. 165, 457–475.
Monecke, T., Gibson, H., Dube, B., Laurin, J., Hannington, M.D., 2008. Geology and volcanic setting of the Horne deposit, Rouyn-Noranda, Quebec: initial results of a new research project. Geological Survey of Canada, Current Research 2008–9 (18 pages).
Morris, R.C., 1980. A textural and mineralogical study of the relationship of iron ore to banded iron-formation in the Hamersley Iron Province of Western Australia. Econ. Geol. 75, 184–209.
Morrison, I.R., 2004. Geology of the Izok Lake massive sulfide deposit, Nunavut Territory, Canada. Explor. Min. Geol. 13, 25–36.
Mortensen, J.K., 1993. U-Pb geochronology of the eastern Abitibi Subprovince. Part 1: Chibougamau-Matagami-Joutel region. Can. J. Earth Sci. 30, 11–28.
Mukhopadhyay, J., Gutzmer, J., Beukes, N.J., Hayashi, K.I., 2008. Stratabound magnetite deposits from the eastern outcrop belt of Archaean Iron Ore Group, Singhbhum craton, India. Trans. Inst. Min. Metall. Sect. B Appl. Earth Sci. 117, 175–186.
Nadoll, P., Mauk, J.L., Hayes, T.S., Koenig, A.E., Box, S.E., 2012. Geochemistry of magnetite from hydrothermal ore deposits and host rocks of the Mesoproterozoic Belt Supergroup, United States. Econ. Geol. 107, 1275–1292.
Nadoll, P., Angerer, T., Mauk, J.L., French, D., Walshe, J., 2014. Ore Geol. Rev. 61, 1–32.
Nesbitt, B.E., 1986. Oxide-sulfide-silicate equilibria associated with metamorphosed ore deposits. Part I: theoretical considerations. Econ. Geol. 81, 831–840.
Nguyen, D., Rocke, D., 2002. Muti-class cancer classification via partial least squares with gene expression profiles. Bioinformatics 18, 1216–1226.
Nielsen, R.L., Forsythe, L.M., Gallahan, W.E., Risk, M.R., 1994. Major- and trace- element magnetite-melt equilibria. Chem. Geol. 117, 167–191.
Pang, K.N., Zhou, M.F., Lindsley, D., Zhao, D., Malpas, J., 2008. Origin of Fe-Ti oxide ores in mafic intrusions: evidence from the Panzhihua intrusion, SW China. J. Petrol. 49, 295–313.
Peter, J.M., Goodfellow, W.D., 1996. Sulphur isotope composition of the Brunswick no. 12 massive sulphide deposit, Bathurst Mining Camp, New Brunswick: implications for ambient environment, sulphur source and ore genesis. Can. J. Earth Sci. 33, 231–251.
Piercey, S.J., Hinchey, J., 2012. Volcanogenic massive sulfide (VMS) deposits of the Central Mobile Belt, Newfoundland. GAC-MAC Joint Annual Meeting 2012, St. Johns, Newfoundland, Field Trip Guidebook- B4 (75 pages).
Piercey, S.J., Paradis, S., Murphy, D.C., Mortensen, J.K., 2001. Geochemistry and paleotectonic setting of felsic volcanic rocks in the Finlayson Lake volcanic-hosted massive sulfide district, Yukon, Canada. Econ. Geol. 96, 1877–1905.
Ray, G., Webster, I., 2007. Geology and chemistry of the low Ti magnetite-bearing Heff Cu-Au skarn and its associated plutonic rocks, Heffley Lake, south-Central British Columbia. Explor. Min. Geol. J. 16, 159–186.
Reich, M., Simon, A.C., Deditius, A.P., Bilenker, L., Knipping, J., Barra, F., 2014. Chemical zoning and microtexture of magnetite from Los Colorados iron oxide-apatite deposit, Chile. Goldschmidt Conference 2014, California, USA.
Rivé, M., Verpaelst, P., Gagnon, Y., Lullin, J.M., Riverin, G., Simard, A. (Eds.), 1990. The Northwestern Quebec Polymetallic Belt. Canadian Institute of Mining and Metallurgy Special Vol. 43 (423 pages).
Riverin, G., LaBrie, M., Salmon, B., Cazavant, A., Asselin, R., Gagnon, M., 1990. The geology of the ansil deposit, Rouyon-Noranda, Quebec. In: Rive, M., Gagnon, P.V.Y., Lulin, J.M., Riverin, G., Simard, A. (Eds.), The Northwestern Quebec Polymetalic Belt. Canadian Institute of Mining, Metallurgy and Petroleum, Special vol. 43, pp. 143–152.
Ross, P.S., McNicoll, V.J., Debreil, J.A., Carr, P.M., 2014. Precise U-Pb geochronology of the Matagami mining camp, Abitibi Greenstone Belt, Quebec: stratigraphic constraints and implications for volcanogenic massive sulfide exploration. Econ. Geol. 109, 89–101.
Savard, D., Barnes, S.J., Dare, S., Beaudoin, G., 2012. Improved calibration technique for magnetite analysis by LA-ICP-MS. Goldschmidt 2012 Abstract.
Shimazaki, H., 1998. On the occurrence of silician magnetites. Resour. Geol. 48, 23–29.
Swinden H.S., and Kean B.F., 1988. The volcanogenic sulphide districts of Central Newfoundland. Geol. Assoc. Can. Guideb., (250 pages).
Taylor, D., Dalstra, H.J., Harding, A.E., Broadbent, G.C., Barley, M.E., 2001. Genesis of high-grade hematite orebodies of the Hamersley province, Western Australia. Econ. Geol. Bull. Soc. Econ. Geol. 96, 837–873.
Tegner, C., Cawthorn, R.G., Kruger, F.J., 2006. Cyclicity in the main and upper zones of the Bushveld Complex, South Africa: crystallization from a zoned magma sheet. J. Petrol. 47, 2257–2279.
Thomas, A., 1978. Volcanic Stratigraphy of the Izok Lake Greenstone Belt, District of Mackenzie, N.W.T. University of Western Ontario (110 pages).
Thurston P.C., and Rogers M.C., 1995. Iron formation: Algoma and Lake Superior types; in Rogers M.C., Thurston P.C., Fyon J.A., Kelly R.I., Breaks, F.W. (comps.), Descriptive Mineral Deposit Models of Metallic and Industrial Deposit Types and Related Mineral Potential Assessment Criteria, Ontario Geological Survey, Open File Report 5916, 76–81.
Toplis, M.J., Carroll, M.R., 1995. An experimental study of the influence of oxygen fugacity on Fe-Ti oxide stability, phase relations, and mineral–melt equilibria in ferro-basaltic systems. J. Petrol. 36, 1137–1170.
Valsami, E., Cann, J.R., 1992. Mobility of rare earth elements in zones of intense hydrothermal alteration in the Pindos ophiolite, Greece. In: Parson, L.M., Murton, B.J., Browning, P. (Eds.), Ophiolites and their Modern Oceanic Analogues. Geological Society, London, Special Publication Vol. 60, pp. 219–232.
van Baalen, M.R., 1993. Titanium mobility in metamorphic systems: a review. Chem. Geol. 110, 233–249.
van Staal, C.R., Ravenhurst, C.E., Winchester, J.A., Roddick, J.C., Langton, J.P., 1990. Evidence for a post Taconic blueschist suture in northern new Brunswick. Geology 18, 1073–1077.
van Staal, C.R., Winchester, J.A., Bédard, J.H., 1991. Geochemical variations in middle Ordovician volcanic rocks of the northern Miramichi highlands and their tectonic significance. Can. J. Earth Sci. 28, 1031–1049.
van Staal, C.R., Fyffe, L.R., Langton, J.P., McCutcheon, S.R., 1992. The Ordovician Tetagouche group, Bathurst camp, northern new Brunswick, Canada: history, tectonic setting, and distribution of massive-sulfide deposits. Explor. Min. Geol. 1, 93–103.
van Staal, C.R., Wilson, R.A., Rogers, N., Fyffe, L.R., Langton, J.P., McCutcheon, S.R., McNicoll, V., Ravenhurst, C.E., 2003. Geology and tectonic history of the Bathurst supergroup, Bathurst mining camp, and its relationships to coeval rocks in southwestern New Brunswick and adjacent Maine- a synthesis. Econ. Geol. Monogr. 11, 37–60.
Von Gruenewaldt, G., Klemm, D.D., Henckel, J., Dehm, R.M., 1985. Exsolution features in titanomagnetites from massive magnetite layers and their host rocks of the upper zone, eastern Bushveld Complex. Econ. Geol. 80, 1049–1061.
Wechsler, B.A., Lindsley, D.H., Prewitt, C.T., 1984. Crystal structure and cation distribution in titanomagnetites ($Fe_{3-x}Ti_xO_4$). Am. Mineral. 69, 754–770.
Westendrop, R.W., Watkinson, D.H., Jonason, I.R., 1991. Silicon-bearing zoned magnetite crystals and the evolution of hydrothermal fluid at the Ansil Cu-Zn mine, Rouyn-Noranda, Quebec. Econ. Geol. 86, 1110–1114.
Westerhuis, J.A., Hoefsloot, C.J.H., Smit, S., Vis, D.J., Smilde, A.K., van Velzen, E.J.J., Duijnhoven, J.P.M., van Dorsten, F.A., 2008. Assessment of PLSDA cross validation. Metabolomics 4 (1), 81–89.
Whitford, D.J., Korsch, M.J., Porritt, P.M., Craven, S.J., 1988. Rare earth element mobility around the volcanogenic polymetallic massive sulfide deposit at Que River, Tasmania, Australia. Chem. Geol. 68, 105–119.
Whitten, E.H.T., 1995. Open and closed compositional data in petrology. Math. Geol. 27 (6), 789–806.
Wishart, D., 2013. Module 6- Backgrounder in Statistical Methods. Informatics and Statistics for Metabolomics Workshop 2013, Toronto, Canada (53 pages).
Wold, H., 1966. Estimation of principal components and related models by iterative least squares. In: Krishnaiaah, P.R. (Ed.), Multivariate Analysis. Academic Press, New York, pp. 391–420.
Wold, S., Sjöström, M., Eriksson, L., 2001. PLS-regression: a basic tool of chemometrics. Chemom. Intell. Lab. Syst. 58 (2), 109–130.
Zaccarini, F., Pushkarev, E.V., Fershtater, G.B., Garuti, G., 2004. Composition and mineralogy of PGE-rich chromitites in the Nurali lehrzolite-gabbro complex. Southern Urals, Russia. Can. Mineral. 42, 545–562.